

# Chapter 1

## INTRODUCTION

The human eye shows such a brilliant design “with all its inimitable contrivances for adjusting the focus to different distances, for admitting different amounts of light, and for the correction of spherical and chromatic aberration” (Darwin, 1859) that it was one of the weak points of Darwin’s evolution theory. The eye, paradoxically, has eventually turned into one of the confirmations of Darwin’s theory (Land and Nilsson, 2002, Nilsson and Arendt, 2008). Helmholtz, aware of the fact that the optics of the eye were far from perfect, also recognized that the eye was so adapted to its function that its limits were set to its defects (Helmholtz, 1885).

Since Helmholtz’s times, technology has advanced to the point of introducing ocular aberrations measurement in clinical environments or making corneal laser refractive surgery an extended alternative for refractive error correction. Knowledge on the aetiology of refractive errors of the eye as well as structural differences across refractive groups has also advanced in the last century. Whereas the exact mechanisms that lead the eye to become ametropic remain unknown, the retinal image is known to have a role in this mechanism (Wallman, 1993, Wildsoet, 1997, Wallman and Winawer, 2004). The aim of this work is to study ametropia in humans, as well as to assess the outcomes of a correction method such as

corneal refractive surgery, using an optical approach, i.e., measurement of ocular aberrations using the laser ray tracing technique (LRT). Additionally, a study of the effect on the estimation of aberrations of different parameters that can be optimised for measurements under particular conditions, such as natural accommodation, is included in this thesis. As an external student, I have carried out this experimental work at Instituto de Óptica (Consejo Superior de Investigaciones Científicas) in Madrid (Spain).

In this introductory chapter a description of the eye is first presented. A short review of the history of aberrometry will follow where the different existing techniques to measure ocular aberrations will be described. Then, the advantages of applying aberrometry to the study of myopia and to assess refractive surgery as a correction method for ametropic eyes will be pointed out. An introduction of the aspects related to aberrometry that will be treated in this thesis will follow: the effect of the interactions of polarisation and wavelength of the light used in the measurement as well as the sampling pattern used to sample the pupil in the estimation of wavefront aberration. Finally, a review of ametropia and the emmetropisation process, followed by a short revision of corneal refractive surgery will complete this chapter.

## **1.1.- THE HUMAN EYE**

Figure 1.1 shows a cross-section of the eye (horizontal section), where it is evident the roughly circular shape of the ocular globe. The axial length of an average adult is approximately 24 mm. The eye is an image forming device, where the cornea and the lens are the optical elements that form a focused image of the outer world on the retina. The refractive power of the eye is about 60 D (Atchison and Smith, 2000).

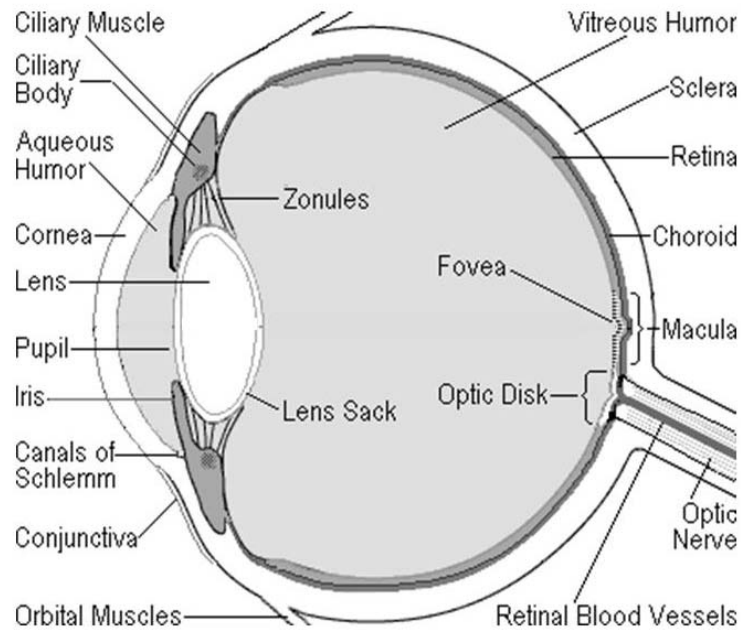


Figure 1.1. Cross-section of the eye (horizontal section) showing the main elements of the eye. Image obtained from <http://www.99main.com/~charlief/Blindness.htm>

### 1.1.1.- CORNEA

The cornea contributes about two-thirds of the power of the relaxed eye ( $\sim 42$  D) (Atchison and Smith, 2000), with anterior and posterior paraxial powers of about  $+49$  D and  $-6$  D, respectively (Charman, 1991b). It forms a meniscus which is thinner in the centre ( $\sim 500$   $\mu\text{m}$ ) than at the edge ( $\sim 700$   $\mu\text{m}$ ), with a refractive index of 1.376 (depending on wavelength and temperature at which it is measured).

Histologically, the cornea can be divided in 5 layers (see Figure 1.2) (Atchison and Smith, 2000): the *epithelium*, in direct contact with the tear film, acts as a barrier against water (to keep corneal transparency) and toxic substances; *Bowman's membrane*, consisting mainly on randomly arranged collagen fibrils; the *stroma*, comprising 90% on the corneal thickness; *Descemet's membrane*, basement membrane of the endothelial cells; and the *endothelium*, consisting on a single layer of hexagonal cells that tile the posterior corneal surface and regulate the corneal hydration in

order to keep transparency. Although the tear film and each corneal layer have their own refractive index (Barbero, 2006), a mean value is usually used ( $n=1.376$ ) (Atchison and Smith, 2000). The optical inhomogeneity of the cornea contributes to the scattering of light that makes it susceptible to be observed in optical section using a slit-lamp or optical coherence tomography (OCT). Of special optical interest is the stroma, and particularly the way the constituent collagen fibres are arranged, which leads to birefringence (see section 1.2.5.1.-) and is crucial to keep corneal transparency, and the mechanical structure of the cornea. The fibres are arranged in approximately regular lattices called lamellae, which are stacked layer upon layer and run from limbus to limbus parallel to the corneal surface, frequently interweaving (Komai and Ushiki, 1991). The orientation of the lamellae is not completely random, but there exists a preferential direction, usually nasal downwards, although there is intersubject variability.

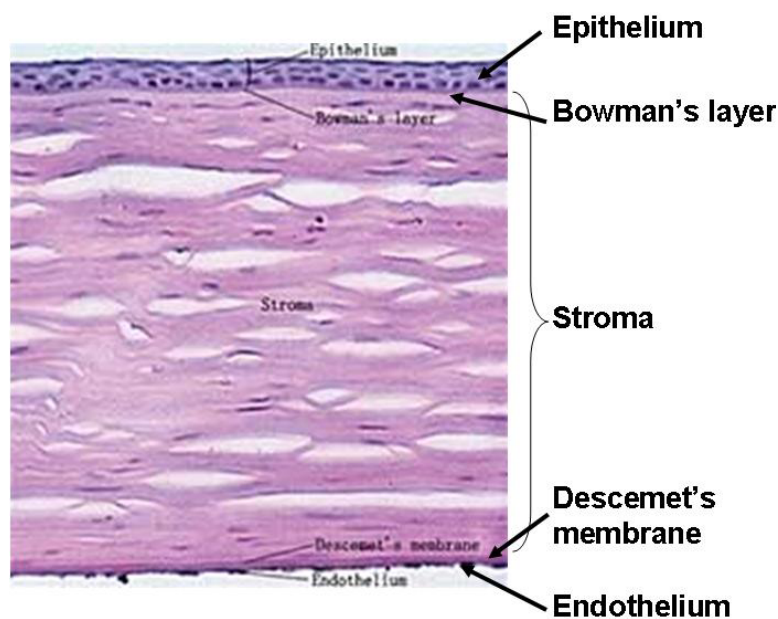


Figure 1.2. Histological section of the cornea showing the different layers. Image from (Yu et al., 2006).

Anatomically, the cornea is oval, its vertical and horizontal diameters being about 12 and 11 mm, respectively. It is continued by the sclera, a dense whitish fibrous layer that gives structure to the eye and that backscatters light strongly (Atchison and Smith, 2000). The cornea is covered by the tear film that, with a thickness of 4-7  $\mu\text{m}$  (Atchison and Smith, 2000), has the optical function of maintaining a smooth optical surface. The anterior corneal surface usually presents different radius at vertical and horizontal meridians (toricity), which produces astigmatism. Generally, in young eyes, the vertical meridian is steeper than the horizontal one, although this tendency reverses with age (Atchison and Smith, 2000). The contour of the anterior cornea can be approximated to a conicoid with rotational symmetry about the z-axis (Kiely et al., 1982), defined by a radius of curvature (CR) and asphericity (Q), which specifies the form of the conicoid. Thus, for  $Q > 0$ , the conicoid is an oblate ellipsoid (major axis parallel to the y-axis), for  $Q = 0$  a sphere, or for  $-1 < Q < 0$  a prolate ellipsoid (major axis along the z-axis) (Figure 1.3). Kiely et al found human corneas to be prolate ellipsoids, i.e., the cornea flattens towards the periphery, with mean CR and Q being  $7.72 \pm 0.27$  mm and  $-0.26 \pm 0.18$ . This asphericity is not enough to compensate for corneal spherical aberration, which is usually positive. Corneas that have suffered LASIK for myopic correction typically present an oblate shape, which results in an increased spherical aberration (see Chapter 7).

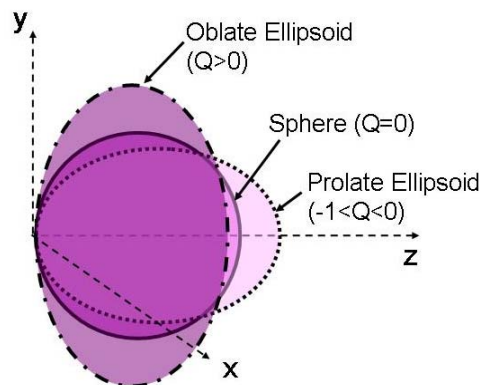


Figure 1.3. Diagram showing the shape of cross-sections of a prolate and an oblate ellipsoids compared to a sphere, according to their asphericity (Q) value.

The posterior corneal surface has a smaller importance in optical terms than the anterior surface due to the smaller index difference in the cornea-aqueous humour interface. In addition, due to the strong influence of the anterior surface, it has been more difficult to measure. Dubbelman et al. (2006) measured the shape of anterior and posterior aging cornea using a Scheimpflug camera (Brown, 1972) and found that the posterior corneal surface had an average radius of  $6.53 \pm 0.25$  mm, the vertical meridian being steeper than the horizontal one, same as for the anterior surface. They also reported that the posterior astigmatism was twice that of the anterior surface. Their posterior Q values varied significantly between meridians, the mean value across the eyes they measured being  $0.48 \pm 0.26$ . With age, the Q of both, anterior and posterior surfaces changed significantly, producing a peripheral thinning.

#### 1.1.2.- CRYSTALLINE LENS

The lens has the shape of a biconvex lens (see Figure 1.4). Different parts can be distinguished (Atchison and Smith, 2000). The lens *capsule* or *sack*, which is a transparent elastic membrane, is attached to the ciliary body by the zonules (see Figure 1.1), and plays an important role in accommodation. Contraction of the ciliary muscle within the ciliary body decreases the tension of the zonules, allowing the lens to take up a more curved shape. This leads to changes in the curvature and index distribution that increase the power of the lens, and therefore of the whole eye to allow focusing near objects. The *lens epithelium* extends from the anterior pole to the equator and it is responsible for the continuous growth of the lens throughout life with new epithelial cells forming at the equator. These cells elongate wrapping the older *fibres*, under the capsule and the epithelium, meeting at the sutures of the lens, originating its characteristic "onion-like" layered structure. The older fibres lose their nuclei and other intracellular organelles, forming a stratified structure of fibre membranes and interstitial cytoplasm (Bettelheim, 1975). The older more central fibres

are squeezed by the younger peripheral ones and have a smaller water content, determining the *nucleus of the lens*, which is less elastic and shows the highest refractive index (about 1.41) (Charman, 1991b). The continuous growth of the nucleus and loss of elasticity is thought to be one of the factors involved on the gradual loss of accommodation with age that leads to presbyopia (complete loss of accommodation) that may occur from 35-40 years. The more peripheral fibres form the *cortex*, which presents the smallest refractive index in the lens (about 1.38). Therefore, the lens has a gradient-index (GRIN), which is thought, together with aspheric surfaces, to reduce spherical aberration. For some purposes, an equivalent refractive index (1.42) is used.

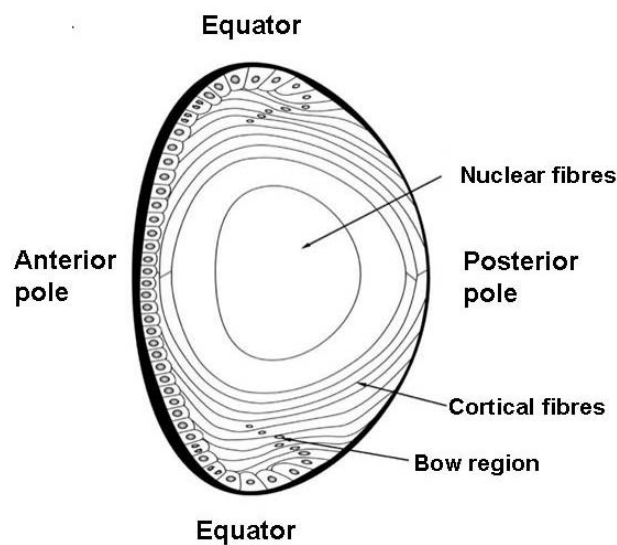


Figure 1.4. Diagram showing a cross-section of the crystalline lens, from (Gupta et al., 2004).

Average ( $\pm$  standard deviation) values of the geometrical parameters of the lens for emmetropic eyes can be found in (Atchison et al., 2008). Reported data for anterior lens radius are  $10.32 \pm 1.41$  mm and  $10.53 \pm 1.40$  mm for males and females, respectively, and for posterior lens radius  $-6.77 \pm 0.78$  mm and  $-6.95 \pm 0.91$  mm for males and females, respectively, all obtained from Purkinje images. Lens central thickness reported values are

4.19 ± 0.47 mm and 4.13 ± 0.40 mm, for males and females, respectively, obtained from ultrasonography. Lens diameter reported values from magnetic resonance imaging (MRI) are 9.21 ± 0.26 mm and 9.31 ± 0.37 mm for males and females, respectively. The reported values of the lens power, obtained from Purkinje images are 23.36 ± 2.09 D and 24.48 ± 2.40 D for males and females, respectively.

### *1.1.3.- CHAMBERS OF THE EYE*

The eye is divided into three chambers: vitreous, anterior and posterior chambers. Anterior and posterior chambers are limited by posterior corneal surface and the iris, and the iris and the crystalline lens anterior surface, respectively (see Figure 1.1). Both chambers are connected by the pupil and filled by the aqueous humour, a transparent liquid with a refractive index about 1.337, very similar to that of the cornea. The aqueous humour is produced in the ciliary processes, at the posterior chamber, and drained at the irido-corneal angle at the anterior chamber. Therefore, it is constantly moving from the posterior to the anterior chamber through the pupil. Under normal conditions it is quite homogenous and does not scatter much light. The vitreous chamber, limited by the posterior surface of the lens and the retina, is the largest chamber in the eye. It is filled by the vitreous body, a transparent gel that fills the vitreous chamber and helps to maintain the structure of the eye. The vitreous body is quite homogeneous and clear, although with age it tends to liquefy and present refractive irregularities (Charman, 1991b).

### *1.1.4.- UVEA*

The uvea is the pigmented vascular layer that lies between the corneoscleral layer and the retina. It consists, from back to front of the eye, of the choroids, the ciliary body and the iris. The iris acts as a variable aperture stop, which controls the amount of light entering the eye and the retinal image quality through its influence on diffraction, aberration and

depth of focus (Charman, 1991b). It can change from about 2 mm to 8 mm in young eyes, but its maximum aperture decreases at old age (miosis). The aperture is called the pupil, and can be artificially dilated (mydriasis) with chemical substances called mydriatics, such as tropicamide. The ciliary body is involved in the accommodation process (see section 1.1.2.-) as well as the production of the aqueous humor (see section 1.1.3.-). The choroid lies behind the retina and due to its high vascularisation and melanin content (Atchison and Smith, 2000) it strongly absorbs short wavelengths and back-scatters long wavelengths (Delori and Pflibsen, 1989).

#### 1.1.5.- *RETINA*

The retina is the light sensitive tissue located at the eye fundus, and connected with the brain through the optical fascicle. The position of the retina in the unaccommodated eye in relation to the focused image projected by the cornea and the lens determines the refractive state of the eye. If the retina is in front of the image, the eye will be hyperopic, and conversely, if it is behind the image, the eye will be myopic. Histologically, it is composed of several cellular and pigmented layers and a nerve fibre layer (see Figure 1.5) that faces the vitreous body and forms the optical fascicle (also called nerve) (see Figure 1.1). Light reaches the retina at the inner limiting membrane, where there is some specular reflection (Atchison and Smith, 2000). The six layers between this and the photoreceptors are highly transparent. The radial arrangement of the fibres in the nerve fibre layer has some effect on polarised light (see Section 1.2.5.1.-). The photoreceptors are the light sensitive cells and are in contact with the retinal pigment epithelium (RPE). Light has to go through the rest of the retinal layers to reach them. There are two kinds of photoreceptors: rods, which are sensitive to low-level light, and the cones, which are wavelength sensitive and are classified as L, M and S depending on whether they are sensitive to long, medium or short wavelengths of the

visible spectrum, respectively. Photoreceptors have wave-guiding properties (Enoch and Lakshminarayanan, 1991). This implies that only light entering each photoreceptor with a particular angle will be guided through it and hence perceived. This also implies that light reflected by the photoreceptors (light in the visible range of the spectrum) will also be guided as opposed to scattered. This will be discussed in section 1.2.5.2.- and Chapter 4. The retinal pigment epithelium (RPE), which is in contact with the choroid, receives this name due to its high content of melanin. Therefore the RPE presents a strong absorption and scatter by melanin granules, although some light passes through it and enters the choroid (Atchison and Smith, 2000). The RPE is involved in the phagocytosis of the outer segment of photoreceptor cells. The residual of this process, a molecule called lipofuscin, accumulates throughout life and has the property of being fluorescent (Delori et al., 1995) (see Chapter 3).

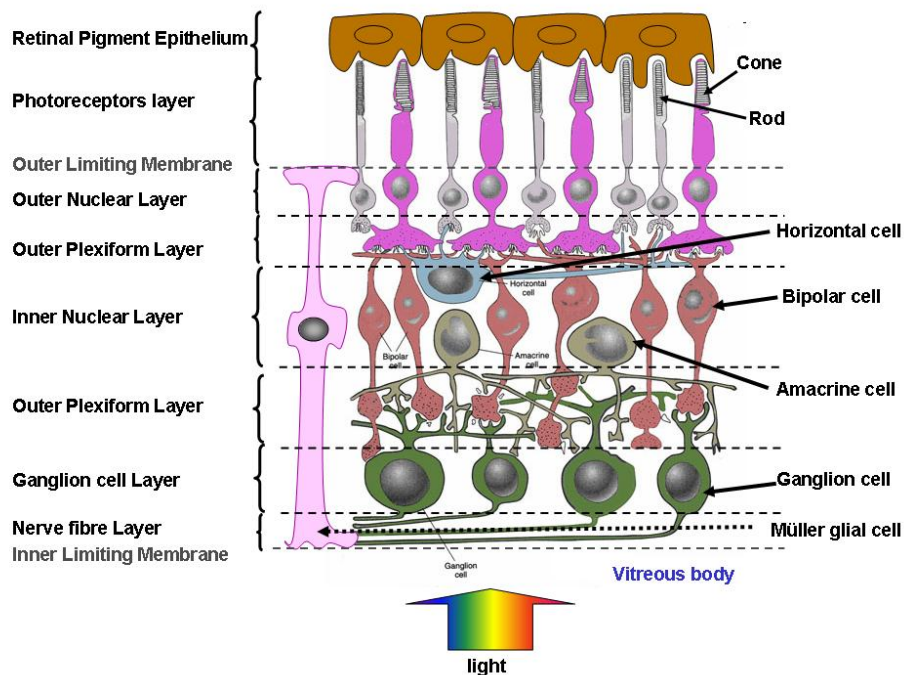


Figure 1.5. Diagram showing the different layers of the vertebrate retina (modified from <http://www.skidmore.edu/~hfoley/images/Retina.jpg>).

Anatomically, two important structures in the retina can be distinguished, the fovea and the optic disk. The fovea (Atchison and Smith, 2000), where cones predominate (no rods exist at its centre), is 1.5

mm wide, and its centre is about  $5^\circ$  from the optical axis (see Section 1.1.6.-). From an optical point of view, the fovea presents an area where the optical aberrations do not change significantly, the *isoplanatic patch*, with a reported diameter of about  $0.80 \pm 0.10^\circ$  (Bedggood et al., 2008). The optic disk (Atchison and Smith, 2000) is approximately  $5^\circ$  horizontally by  $7^\circ$  vertically. With its centre located approximately  $15^\circ$  nasally and  $1.5^\circ$  upwards from the fovea, it is the region where vascular supply enters the eye and the optic fascicle leaves the eye. Therefore there are no photoreceptors in this region, and because of that the corresponding region in the visual field is called *blind spot*.

### 1.1.6.- AXIS OF THE EYE

The eye is not a centred, rotationally symmetric optical system: the curvature centres of the ocular surfaces as well as the fovea do not lie in a single common axis (Atchison and Smith, 2000). Because of this, different axes are defined for the eye. The *optical axis* of the eye is defined as the line joining the centres of curvature of the anterior cornea and the posterior lens surfaces. The *line of sight* is the line joining the fixation point and the centre of the entrance pupil of the eye, and is the reference that will be used for the ocular aberrations maps (see section 1.2.1.-). The keratometric axis is that used in keratometers or corneal topographers and contains the centre of curvature of the anterior cornea, usually intercepting the line of sight at the fixation point.

## 1.2.- ABERROMETRY

### 1.2.1.- OPTICAL ABERRATIONS

There are different methods to specify the image quality yielded by an optical system. The approach usually applied to describe the optical performance of the eye, is in terms of the wave aberration (see Figure 1.6). The wave aberration,  $W(x,y)$ , describes the distortions of the wavefront as

it goes through an optical system. A mathematical description of the electromagnetic waves can be found in Born and Wolf (1993). The wavefront is the surface containing the points of a wave on the same phase, which are orthogonal to the corresponding ray pencils. Therefore, if an aberrations-free optical system forms a perfect point image, all the imaging rays will intersect this point to form the image, or equivalently, all the imaging wavefronts will be spherical, centred on the image point. Under these conditions the optical system will be estigmatic and the image of a point source will be a point. However, when the optical system is aberrated there is no longer a point focus: the rays will not intersect on a single point, and the wavefronts will no longer be spherical. When the system forms a perfect image focused at infinity, the rays will be parallel, and the wavefronts will be planes (spheres of infinite radius). Thus, the aberration can be described in terms of the distance that each point of the wavefront departs from the ideal sphere at the exit pupil (Charman, 1991b). Wave aberration can be represented in a wave aberration map as shown in Figure 1.6, where the colour indicates the distance between the wavefront and the reference sphere, and the lines join points at equal distance. Therefore, optical aberrations can be represented as: wave aberration (departure of the wavefront from the ideal wavefront, as measured at the exit pupil), transverse aberration (departure of a ray from its ideal position at the image plane), or longitudinal aberration (departure of the intersection of a ray with the optical axis from its ideal position) (Atchison and Smith, 2000).

Optical aberrations can be divided in chromatic and monochromatic (geometrical) aberrations. Chromatic aberrations are a consequence of the dispersion (variation of refractive index with wavelength) of the refractive media of an optical system. There are two types of chromatic aberrations. The *longitudinal* chromatic aberration (LCA) is produced because different wavelengths are focused at different image planes, and can be quantified as the variation in power with wavelength. The *transverse* chromatic

aberration (TCA) is produced when obliquely incident rays are focused at different transverse positions within the image plane.

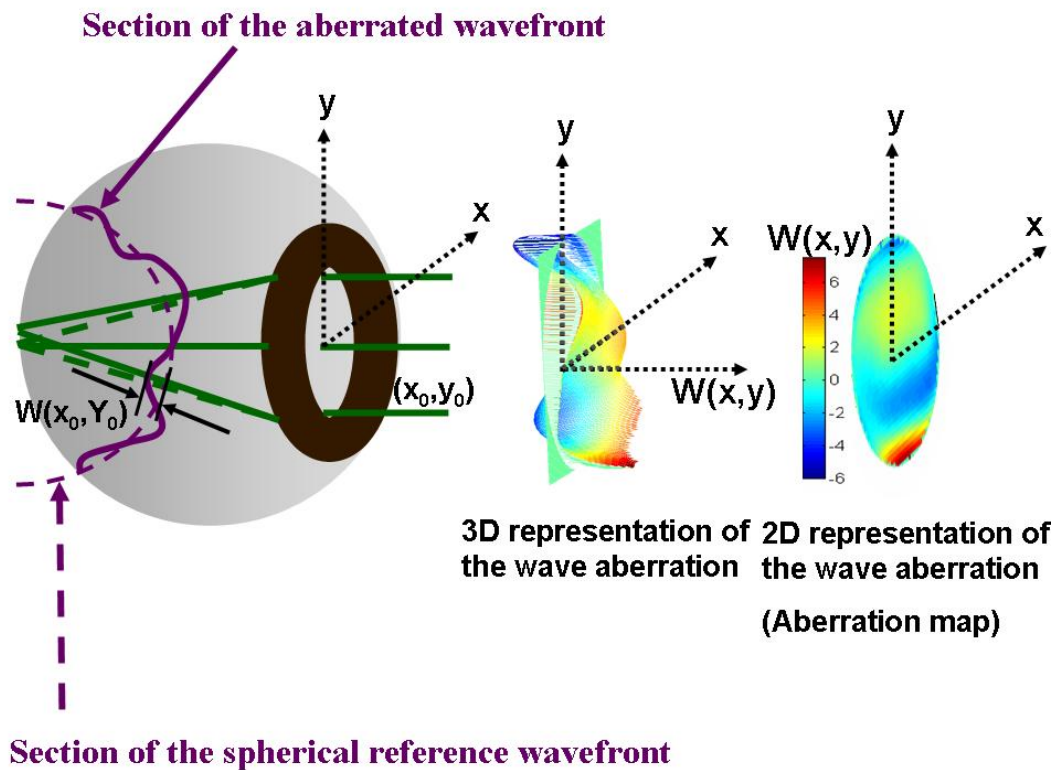


Figure 1.6. Schematic representation of the wave aberration. Wave aberration values (distances between the distorted aberrated wavefront and the spherical reference) can be represented as  $z$ -coordinate referred to the pupil plane (three-dimensional representation) or can be represented as a colour gradation (Aberration map).

Monochromatic aberrations are those present when only one wavelength is considered, and arise from the geometry, irregularities, tilts and decentrations of the components of the optical system. The magnitude of the geometrical aberrations increases with the diameter of the exit pupil considered. Seidel (Seidel, 1856) named in 1856 the seven primary aberrations, which include, apart from the chromatic aberrations, five monochromatic aberrations: Astigmatism, Spherical aberration, Coma, Field Curvature and Distortion. In the presence of any of the first three aberrations, the optical system will not be able to image a point source as a point, and the resulting image will be blurred, degrading the retinal image. When astigmatism is present, parallel rays are focused down to two mutually perpendicular focal lines at different positions (see Figure

1.7 A). Astigmatism is usually due to lack of symmetry of at least one surface, usually the anterior cornea in the eye (Atchison and Smith, 2000). Positive (negative) spherical aberration is present when parallel non-paraxial rays do not intersect at the paraxial focus, but in front or behind it (see Figure 1.7 B). The further the ray is from the optical axis, the greater this effect will be. Spherical aberration (SA) is rotationally symmetric and depends on the radius of curvature (R) and on the asphericity (Q) of the optical surfaces (SA decreases when R increases and increases with Q). In a rotationally symmetric system, coma is an off-axis aberration, where rays departing from an off-axis point reach the image plane at different points (see Figure 1.7 C). In the eye, coma-like aberrations present at the fovea are the result of the lack of symmetry of the optical elements around an optical axis (Atchison and Smith, 2000). Field curvature and distortion are also off-axis aberrations. In both cases a source point is imaged as a point, but the position will be different from that predicted from paraxial optics: when field of curvature is present the point will be imaged in front of (for systems with components of positive power such as the eye) or behind the paraxial focal plane, and when distortion is present, the point is formed in the paraxial image plane but further away (positive distortion) or closer (negative distortion) to the optical axis than expected (Atchison and Smith, 2000).

Piston, tilt and defocus are not considered Seidel aberrations, although tilt and defocus have the same dependence with pupil coordinates as distortion and field of curvature, respectively. Piston is the mean value of the wavefront across the pupil of an optical system, and tilt quantises the average slope of the wavefront in X and Y directions (Malacara, 1992). Defocus occurs when parallel rays (paraxial and not paraxial) converge in front of (positive defocus) or behind (negative defocus) the paraxial focus. Although not considered a Seidel aberration, defocus is considered a low order aberration when the wave aberration is described in terms of a polynomial series.

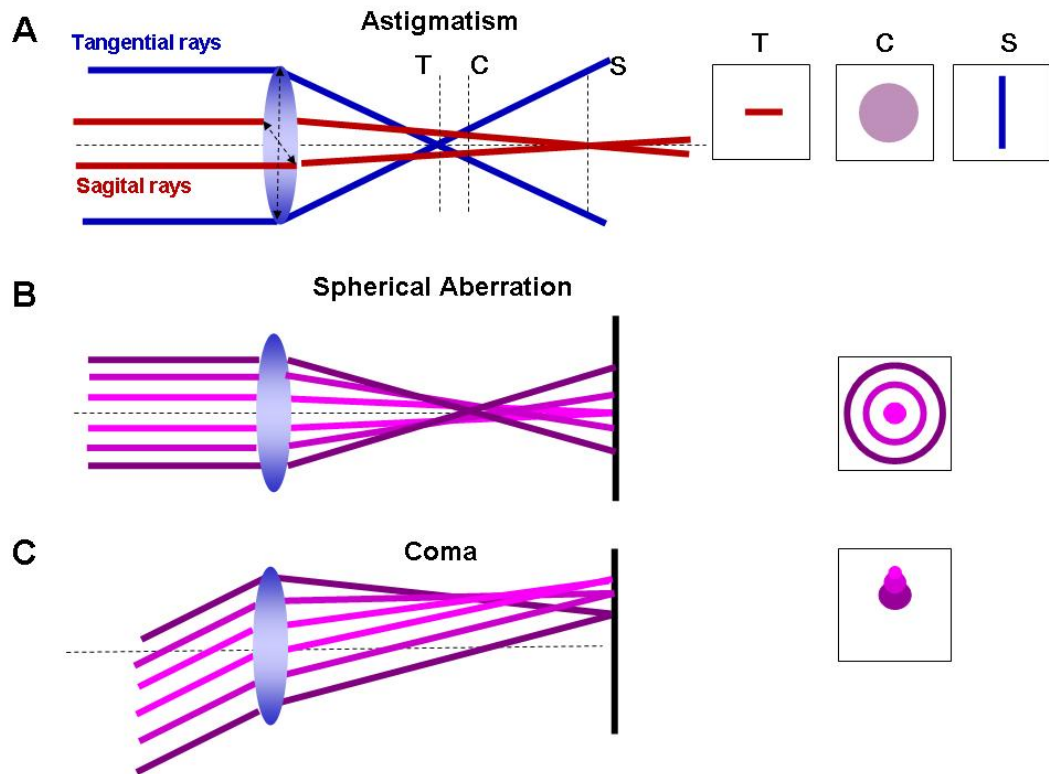


Figure 1.7. Illustration of those Seidel aberrations which prevent optical systems from forming a point image from a point object: astigmatism (A), spherical aberration (B) and coma (C). T, S, and C stand for the image planes corresponding to tangential rays, sagittal rays and circle of minimum confusion.

Apart from the optical aberrations, other retinal image quality criteria are commonly used, such as the point-spread function (PSF) and the Modulation Transfer Function (MTF). The PSF is the illuminance distribution of a point source of light in the image, and its shape depends on diffraction, defocus, aberrations and scatter. The PSF produced by the optical aberrations is proportional to the Fourier transform of the wave aberration function. The MTF quantifies how each spatial frequency is transferred by an optical system by measuring the amplitude of the output (image) for each spatial frequency in relation to an input (object) of known amplitude (de Valois and de Valois, 1988). The MTF can be calculated as the magnitude of the autocorrelation of the wave aberration function (Atchison and Smith, 2000). The quality of the visual system depends not only on optical factors, but on neural factors such as sizes and spacing of

retinal cells, the degree of spatial summation at the different levels from the retina to the visual cortex and higher level processing (Atchison and Smith, 2000). The Contrast Sensitivity Function (CSF) measures the contrast required by an observer for the detection of each of different spatial frequencies, and is expressed as the reciprocal of the contrast required for detection (de Valois and de Valois, 1988). It hence includes optical as well as neural factors. The MTF and the reciprocal of the CSF are therefore closely associated (Atchison and Smith, 2000).

### 1.2.2.- ESTIMATION OF ABERRATIONS

The wave aberration of a general optical system can be described mathematically by a polynomial series. Although some other polynomial series have been proposed (Howland and Howland, 1977), Zernike polynomial (Born and Wolf, 1993) expansion has become the standard for representing ocular wave aberration data, since they present some advantages for this purpose: 1) they are defined over the unit circle, and aberrations are usually referred to circular pupils; and 2) some terms can be easily related to Seidel aberrations (Born and Wolf, 1993). Therefore, a wave aberration can be described as a summation of Zernike polynomial functions weighted by the so-called Zernike coefficients, which indicate the magnitude of each particular aberration present:

$$W(X,Y) \approx \sum_n \sum_m C_n^m Z_n^m(X,Y) \quad (1.1)$$

where  $W(X,Y)$  is the wave aberration phase in microns as a function of cartesian coordinates,  $C_n^m$  and  $Z_n^m(X,Y)$  are the Zernike coefficient in microns and Zernike polynomial (dimensionless), respectively, as a function of cartesian coordinates, corresponding to the radial order  $n$  and the meridional frequency  $m$  (see Figure 1.8). The Optical Society of America established a set of recommendations regarding sign, normalisation and ordering that will be followed

throughout this work (Thibos et al., 2000). A mathematical definition of the Zernike polynomials according to these recommendations can also be found in the same reference. Following this convention,  $W > 0$  means the wavefront is phase-advanced relative to the chief ray. Figure 1.8 shows the three-dimensional representation of the Zernike polynomials up to 6<sup>th</sup> order with the corresponding names and notation. As can be observed from the figure, terms with meridional frequency zero are rotationally symmetric. The Root Mean Square wavefront error (RMS), defined as “the root square of the sum of the squares of the optical path differences as measured from a best-fit reference spherical wavefront over the total wavefront area” (Fischer et al., 2007), is typically used as a global metric for the optical quality.

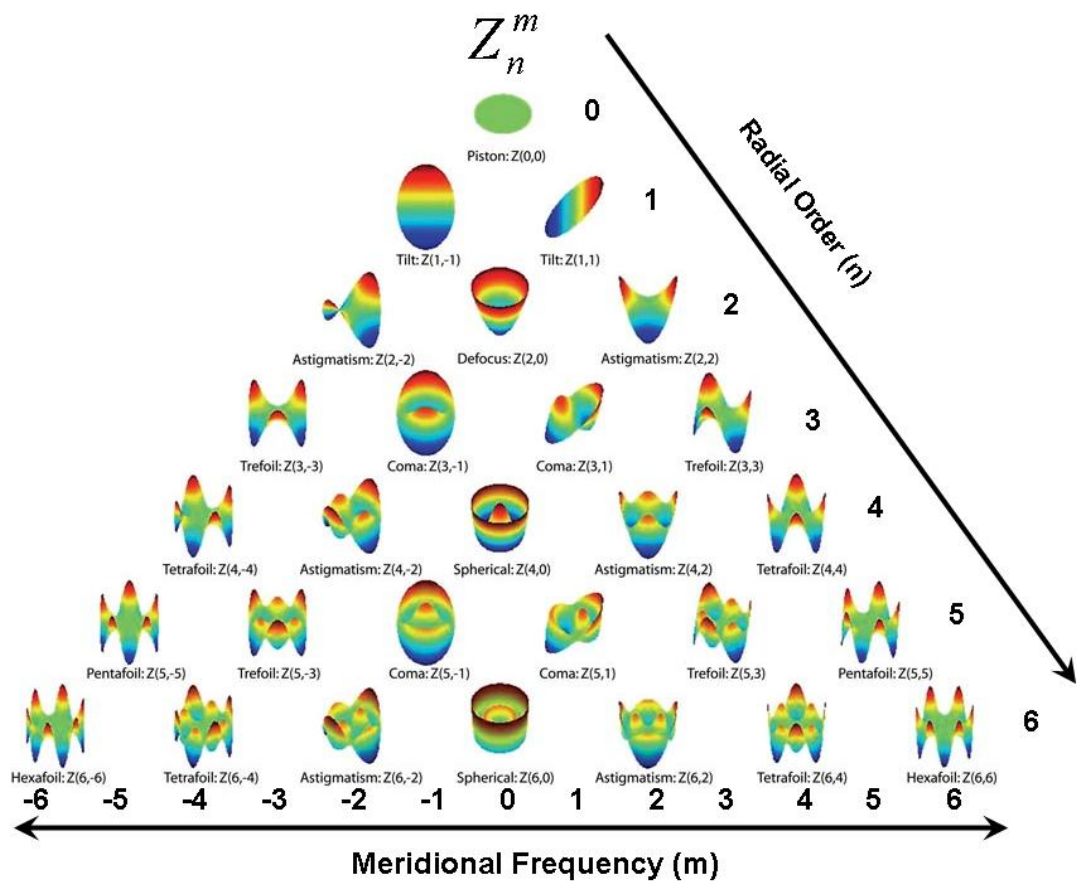


Figure 1.8. Representation of the Zernike base functions. Each row in the pyramid corresponds to a radial order of the polynomial, and each column to a meridional frequency. Positive and negative frequencies indicate harmonics in cosine and sine phase, respectively. Negative frequency astigmatism and  $n$ -foil terms are usually denominated “oblique” astigmatism or  $n$ -foil. Positive and negative frequency coma terms are usually denominated as horizontal or vertical coma, respectively. Although each mode can be assigned a single reference number, a double-script notation which designates each basis function according to its order (subscript) and frequency (superscript) is commonly used (Thibos et al., 2000).

Most methods of estimation of the wave aberration are based on local sampling of the pupil and measurement of the local wave aberration slope. The local slope (partial derivatives) of the wavefront is proportional to the ray aberration (Born and Wolf, 1993):

$$\Delta x' = \frac{1}{R_p} \frac{\partial W(\bar{\xi}, \bar{\eta})}{\partial \bar{\xi}}; \quad \Delta y' = \frac{1}{R_p} \frac{\partial W(\bar{\xi}, \bar{\eta})}{\partial \bar{\eta}} \quad (1.2)$$

where  $\bar{\xi} = \xi / R_p$ ,  $\bar{\eta} = \eta / R_p$  are dimensionless canonical pupil coordinates and  $R_p$  is the pupil radius (Moreno-Barriuso et al., 2001a).

The wave aberration is reconstructed by integrating the slopes of an array of beams intersecting the eye's entrance (or exit in some cases) pupil (Howland, 2000). This reconstruction can be local (Southwell, 1980), modal (Cubalchini, 1979, Rimmer, 1974, Fried, 1977, Herrmann, 1981) (or a mixture of both), if the estimate is a phase value on a local area or a coefficient of an aperture function (Southwell, 1980). Usually, in any case a least-square estimation is used for phase reconstruction. Some questions to consider when selecting the reconstruction model are the compatibility with the sampling geometry of the sensor, the reconstruction algorithm complexity (convergence problems, computation speed requirements), and the propagation error. The most widely used method in ocular aberrometry is a modal reconstruction that is based on the expansion of the derivatives of wave aberration as a linear combination of a set of base functions (most frequently the derivatives of Zernike polynomial expansion), and a subsequent least-squares fit of the expansion coefficients to the measured gradients (Rios et al., 1997). Southwell (Southwell, 1980) found that modal estimation was superior to zonal estimation in terms of noise propagation, particularly when only a fixed number of modes were of interest, and that modal estimation was computationally easier and faster. These advantages enhanced as the number of samples increased. Regarding the compatibility with the geometry of the sensor, some geometries not currently being used might be better adapted to the

geometry of Zernike functions (see Section 1.2.5.3.-). This topic will be addressed in Chapter 5 of this thesis.

### 1.2.3.- HISTORY AND TYPES OF ABERROMETERS

The history of aberrometry dates back to 1619 when Scheiner (Scheiner, 1619 in Biedermann, 2002) invented a disk with a central and a peripheral pinhole that was placed in front of the eye of a subject, so that an imperfect eye would form two retinal images when looking at a distant point light source. Helmholtz (1821-1894) was one of the pioneers who extensively investigated the structure of the human eye, including its aberrations. He foresaw that human ocular aberrations were significant enough to degrade the retinal image (Helmholtz, 1885). Around the same time, in 1894, Tscherning (Tscherning, 1894 in Biedermann, 2002) built what he called "an aberroscope" to measure human eye aberrations, consisting on a grid superimposed on a 5-diopter lens so that the image of the grid was shadowed on the subject's retina when viewing a distant point light source through the "aberscope". Aberrations were estimated from the distortions of the grid. In 1900 Hartmann (Hartmann, 1900 in Biedermann, 2002) used Scheiner's idea to measure aberrations in mirrors and lenses, using an opaque screen perforated with numerous holes, which is commonly referred to as wavefront sensor. Independently Smirnov (Smirnov, 1961), in 1961 had the idea of sequentially rotating Scheiner's disk in order to sample the whole pupil. One year before B. Howland (Howland, 1968) had invented the crossed cylinder aberroscope, a modification of Tscherning's one that used a crossed cylinders lens, that he used to study aberrations in camera lenses. It was not until a few years later that it was applied to measure aberrations of the human eye subjectively (Howland and Howland, 1976), with the subject drawing the perceived distorted grid. In 1984, Walsh et al. (1984) turned Howland's aberroscope into an objective method by photographing the image of the grid on the retina. In 1971 Shack and Platt (Shack and Platt, 1971)

improved Hartmann's screen by using an array of microlenses (or lenslets) instead of the perforations to analyse the wavefront coming out of the optical system to study. The array of microlenses is called a Hartmann-Shack (HS) wavefront sensor, and it is composed of a number of microlenses with the same focal length, arranged in a known geometry. A diagram of the working principle of a HS is shown in Figure 1.9. In this technique (Liang et al., 1994), a point source is created in the object space, at the fovea. Light from the eye reaching each lenslet is brought to a focus in the focal plane of the lens array. When an ideal plane wave reaches the sensor, the image obtained in its focal plane reproduces the geometry of the sensor, given that each spot is located on the optical axis of the corresponding lenslet. The pattern of spots in this image will be used as a reference. When an aberrated wavefront is measured, the image spot produced by each lenslet shifts with respect to the corresponding point in the reference a distance proportional to the local phase distortion (transverse aberration). The HS sensor was first applied in astronomy. It was in 1994 when it was adapted by Liang et al (Liang et al., 1994) in Heidelberg for measuring aberrations of the eye, and a couple of years later it was developed in Rochester and integrated in an adaptive optics flood illumination fundus camera to image the human eye retina with unprecedented resolution by removing the eye aberrations using a deformable mirror (Miller et al., 1996). In this thesis a HS sensor has been used to measure ocular aberrations in Chapters 3 and 4.

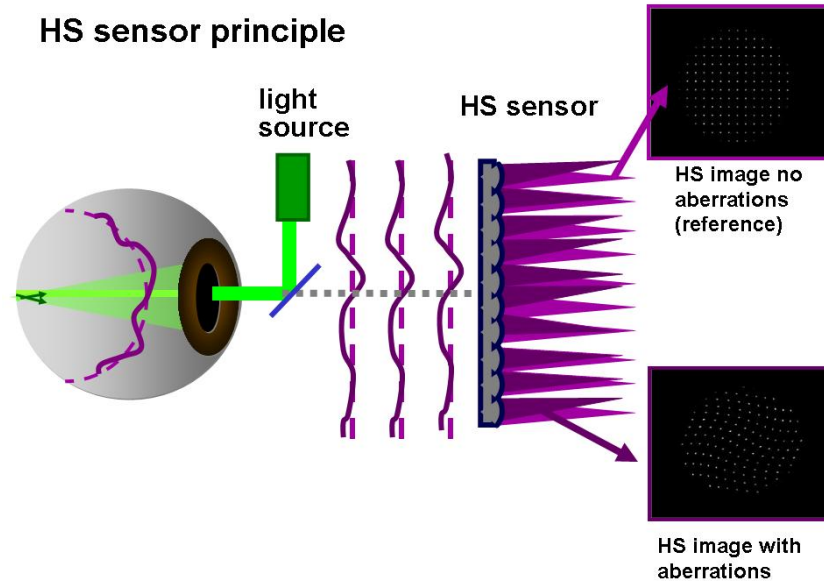


Figure 1.9. Diagram of the working principle of Hartmann-Shack (SH) sensor. A point source at the retina emits spherical wavefronts which are distorted by the eye aberrations. Each lenslet will sample a portion of the wavefront on a different phase, and will form a point image away from its focal point a distance proportional to the phase distortion. Modified from original by S. Marcos.

Some years later, the Ray Tracing technique (LRT) (Navarro and Losada, 1997, Molebny et al., 1997) was applied to measure ocular aberrations. This technique, which has been used throughout this thesis will be more extensively described in Chapter 2, section 2.2. A diagram of the working principle of LRT is shown in Figure 1.10. Collimated laser pencils are sequentially delivered through different pupil positions, so that each pencil will be deviated an angle proportional to the local wave aberration, and will impact at a foveal location away from that of the reference central ray (transverse aberration). The joint plot of the impacts corresponding to the rays entering through different pupil locations is a spot diagram. There is a psychophysical version of the ray tracing, the Spatially Resolved Refractometer (SRR), where the ray aberration at each pupil point is computed as the angle that the subject has to tilt the incoming beam in order to visualize the ray centred on the retina (Webb et al., 1992, He et al., 1998). Some aberrometers measure the ray aberration on the retina or image space ("ingoing" techniques), i.e., they measure the deviation of the rays as they enter the eye. This is the case of the LRT, SRR or Tscherning's type aberrometer (Seiler et al., 2000) previously described.

In other aberrometers, aberrations are measured in the object space (“outgoing” techniques), i.e., as the light exit the eyes. This is the case of the Hartmann-Shack technique. Table 1.1 compares the different aberrometry techniques according to some of their features.

### LRT principle

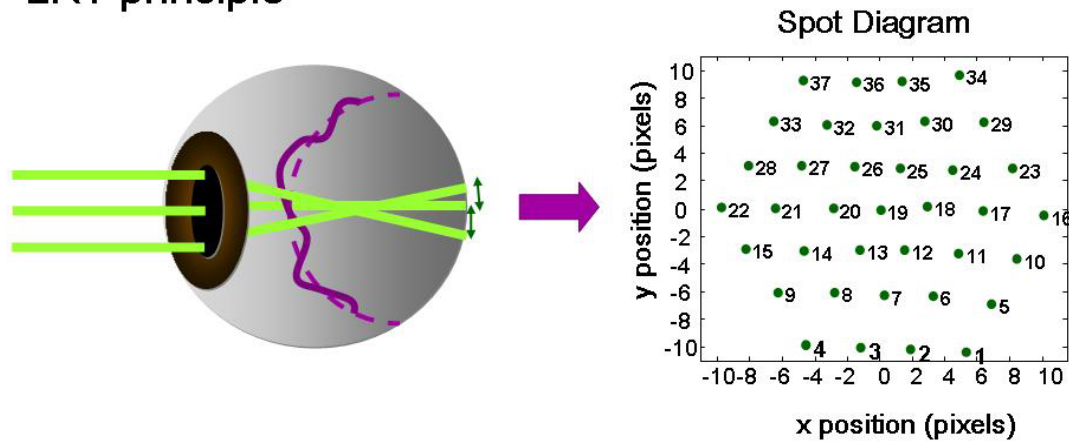


Figure 1.10. Schematic diagram showing the working principle of Laser Ray Tracing (LRT): parallel rays sequentially delivered through different pupil positions deviate an angle proportional to the wave aberration will impact at a different foveal location. A spot diagram can be represented by plotting jointly the impacts sequentially collected for all the pupil locations. Modified from an original diagram by S. Marcos.

COMPARISON	HS	Tscherning	LRT	SRR
Method type	Objective	Objective	Objective	Psychophysical
Configuration	Parallel	Parallel	Sequential	Sequential
Flexibility	“Rigid” configuration	“Rigid” configuration	Configurable sampling pattern	Configurable sampling pattern
Measurement Step	Measurement in 2 <sup>nd</sup> step (“outgoing”)	Measurement in 1 <sup>st</sup> step (“ingoing”)	Measurement in 1 <sup>st</sup> step (“ingoing”)	Measurement in 1 <sup>st</sup> step (only) (“ingoing”)
Pixels per centroid Range	Few pixels	Few pixels	Whole sensor	Whole sensor
Test size on retina	Foveal	Extensive	Foveal	Foveal
Measurement time range	milliseconds	milliseconds	seconds	minutes

Table 1.1. Comparison of the features of the different techniques to estimate ocular aberrations from transverse aberrations.

In this work, the LRT technique to measure ocular aberrations has been mainly used. This technique has a large dynamic range and can measure largely degraded eyes given that, since images are captured sequentially, the entire CCD sensor is available for each aerial image. This makes LRT well-suited to study eyes with optical quality varying widely in magnitude in a wide range, as will be explained in section 1.2.6.-. The flexibility in its configuration has allowed us to carry out experiments that would have been more challenging with other techniques, such as the work described in Chapter 5. Finally, this objective method allows shorter measuring times compared to its psychophysical counterpart (SRR).

#### *1.2.4.- OPTICAL ABERRATIONS OF THE HUMAN EYE*

Ever since Helmholtz foresaw that the eye, far away from being a perfect optical system, presented even more optical aberrations than the optical instruments at the time (Helmholtz, 1885), the measurement of aberrations has advanced to the point that there exist several studies characterising the aberrations of the general population and aberrometers have become available in the clinical practice. In this section a description of the characteristics of the aberrations pattern which are common among the normal population is presented. An overview of current knowledge of the aberrations of the entire eye will be presented, followed by the aberrations of the cornea and finally discuss the interaction of corneal and internal aberrations to yield the overall ocular aberrations pattern.

##### *1.2.4.1.- Ocular Aberrations*

Early studies on the ocular (total) aberrations of the human eyes (Von Bahr, 1945, Van Heel, 1946, Ivanoff, 1953, Smirnov, 1961, Van der Brink, 1962, Jenkins, 1963, Howland and Howland, 1976, Howland and Howland, 1977) already reported a large variation of the magnitude and distribution of the aberrations among individuals, which has been confirmed by later studies including a larger number of eyes. In addition,

optical aberrations are known to change with age (see below), be related to the refractive group of the eye (see section 1.3.1.-) and depend on the pupil size. However, some general conclusions across the population can be extracted.

1) The defocus Zernike term, followed by both astigmatic terms (second Zernike order), are the main contributors to the total RMS (Porter et al., 2001, Castejon-Mochon et al., 2002, Thibos et al., 2002, Cheng et al., 2004);

2) In general, for each subject, the magnitude of the aberrations decreases as the Zernike order increases (Porter et al., 2001, Castejon-Mochon et al., 2002, Thibos et al., 2002, Cheng et al., 2004), with terms beyond fourth Zernike order being practically zero (Castejon-Mochon et al., 2002, Cheng et al., 2004). Fourth order SA ( $Z_4^0$ ) has been reported to be larger in magnitude than the previous third order terms (Porter et al., 2001, Castejon-Mochon et al., 2002, Thibos et al., 2002). However, some studies also report third order aberrations (coma and trefoil) to dominate the HOA pattern of normal eyes (Howland, 2002, Applegate et al., 2007).

3) The average value of each term across the population is zero, except for 4<sup>th</sup> order SA ( $Z_4^0$ ), which has been found to be significantly positive across subjects, with reported values including, for example, 0.037  $\mu\text{m}$  (6 mm pupil) (Plainis and Pallikaris, 2006),  $0.065 \pm 0.083 \mu\text{m}$  (5 mm pupil) (Cheng et al., 2004),  $0.128 \pm 0.096 \mu\text{m}$  (6 mm pupil) (Salmon and de Pol, 2006) and 0.138  $\mu\text{m}$  (5.7mm pupil) (Porter et al., 2001). These values depend on characteristics of the studied population such as age and refractive error. However, Plainis et al. reported that also oblique trefoil ( $Z_3^{-3}$ ) was significantly different from zero with an average value of -0.062  $\mu\text{m}$ . Data reported by Salmon and de Pol (2006) support this finding (they report a mean value of 0.11  $\mu\text{m}$ ), and include vertical coma ( $Z_3^{-1}$ ), with a mean value of 0.14  $\mu\text{m}$ , among the most prominent Zernike terms.

4) The aberrations of the eye seem to be related in such a way that the overall optical quality of the eye was optimised (McLellan et al., 2006). This feature was not found for corneal aberrations or for randomly generated sets of aberrations with the same RMSs as the measured eyes.

5) The reported average RMS for HOA in a large young normal population is 0.22  $\mu\text{m}$  (5 mm pupil) (Cheng et al., 2004), 0.26  $\mu\text{m}$  (6 mm pupil) (Plainis and Pallikaris, 2006) and 0.33  $\mu\text{m}$  (6 mm pupil) (Salmon and de Pol, 2006).

6) A bilateral symmetry in the aberration patterns corresponding to both eyes of the same subject has been reported (Castejon-Mochon et al., 2002, Marcos and Burns, 2000, Plainis and Pallikaris, 2006, Thibos et al., 2002, Porter et al., 2001, Kelly et al., 2004). Aberration patterns from both eyes present a mirror symmetry, which is confirmed by negative correlations found between left and right eyes for most of the Zernike coefficients corresponding to asymmetric Zernike functions such as coma and astigmatism (Porter et al., 2001). The highest correlation between Zernike terms was found for defocus, followed by SA and astigmatic terms (Porter et al., 2001, Castejon-Mochon et al., 2002).

Ocular aberrations have been reported to increase with age (Applegate et al., 2007, Artal et al., 2002, McLellan et al., 2001, Calver et al., 1999) for a fixed pupil diameter, and in particular, the RMS for HOA has been found to increase significantly (McLellan). A change in SA with age towards positive values, attributed to a loss of the compensation between the cornea and the crystalline lens (Artal et al., 2001, He et al., 2003, McLellan et al., 2001, Smith et al., 2001, El Hage and Berny, 1973, Radhakrishnan and Charman, 2007, Millodot and Sivak, 1979), has also been found. Salmon et al. (2006) found a gradual increase of SA with age, although the wide variability they found indicated the influence of other factors than age. Recent studies in emmetropic eyes (Atchison et al., 2008, Plainis and Pallikaris, 2006) did not confirm this change, suggesting that

interactions between age and refraction might have influenced the results of previous studies. Third order aberrations have also been reported to increase with age (McLellan et al., 2001), particularly horizontal coma ( $Z_3^1$ ) (Atchison et al., 2008, Salmon and de Pol, 2006). Salmon et al. (2006) also found correlations for terms  $Z_3^{-1}$ ,  $Z_4^2$  and  $Z_4^4$ . McLellan et al. found a strong significant positive correlation between 5<sup>th</sup> and higher order aberrations RMS and age, and Salmon et al. found significant correlations for 3<sup>rd</sup>, 4<sup>th</sup>, 5<sup>th</sup> and 6<sup>th</sup> RMSs.

#### 1.2.4.2.- Corneal Aberrations

Given that the cornea contributes about two-thirds of the power of the relaxed eye (Atchison and Smith, 2000), it has a great influence in the ocular aberrations. Currently, the most extended way to estimate anterior corneal aberrations is from the elevation maps obtained from a corneal topographer in combination with ray tracing through the optical surface defined by these maps (Applegate et al., 1996, Barbero et al., 2002b, Guirao and Artal, 2000). Similarly to ocular aberrations, corneal aberrations have been reported to vary widely among the population (Guirao et al., 2000, Wang et al., 2003b), and apparently corneal aberrations also present some bilateral symmetry (Wang et al., 2003b, Lombardo et al., 2006). The anterior cornea presents with-the-rule astigmatism (vertical meridian steeper), which generally reverses with age into against-the-rule, and positive SA. Wang et al. (2003b) reported average values of  $0.280 \pm 0.086$   $\mu\text{m}$ ,  $0.248 \pm 0.135$   $\mu\text{m}$  and  $0.479 \pm 0.124$   $\mu\text{m}$  for SA, coma and HOA, respectively for a population ranging from 20 to 79 years old (mean age was 50 years). In terms of aging, anterior corneal aberrations have been reported to increase moderately with age (Oshika et al., 1999a, Guirao et al., 2000, Atchison et al., 2008). Particularly, third order coma has been found to increase with age (Oshika et al., 1999a, Guirao et al., 2000). However, Atchison et al. only found a significant increase in the 6<sup>th</sup> order

terms, apart from HOA. The reason might be the interaction between age and refraction previously commented.

The posterior corneal surface has a smaller effect on HOA of the eye (Dubbelman et al., 2007), due to the small index difference between the cornea and the aqueous humour (Atchison and Smith, 2000). Using a distortion corrected Scheimpflug camera (Brown, 1972), Dubbelmann et al. (2006) found a compensation of 31% of the anterior corneal astigmatism by the posterior cornea. Using the same technique, Sicam et al. (2006) found that SA of the posterior cornea is negative in young eyes and becomes positive with age, disrupting the compensation of the positive SA of the anterior cornea. Dubbelman et al. (2007) also found a coma compensation of 3.5% between both corneal surfaces, that disappeared with age.

#### *1.2.4.3.- Internal Aberrations: interaction between total and corneal aberrations*

Internal aberrations can be estimated from the subtraction of anterior corneal aberrations from ocular (total) aberrations, and include the aberrations of the lens and the posterior cornea (as the humours are not believed to play a significant role in terms of aberrations). Knowledge of the relative contribution of the cornea and the lens to the ocular wave aberration is important for both, basic study of the human eye and clinical applications, as will be shown in Chapters 6 and 7, respectively.

The existing compensation of the positive corneal SA by the negative SA of the lens has been reported since the 70's (El Hage and Berny, 1973, Millodot and Sivak, 1979), and has been confirmed since, using different techniques (Tomlinson et al., 1993, Smith et al., 2001, Artal and Guirao, 1998, Artal et al., 2001, Barbero et al., 2002a, Kelly et al., 2004). This compensation had also been reported for astigmatism (Le Grand and El Hage, 1980, Artal et al., 2001, Kelly et al., 2004) and is quite well known in clinical practice. The development of techniques to measure the aberrations

has allowed the initial studies on astigmatism and SA compensation to be expanded to other aberrations. Artal et al. (2001) found compensation in both astigmatism Zernike terms, SA, oblique trefoil and coma. Kelly et al. (2004) confirmed Artal's findings for horizontal/vertical astigmatism ( $Z_2^2$ ), horizontal coma ( $Z_3^1$ ) and SA ( $Z_4^0$ ), but they did not find compensation for oblique trefoil ( $Z_3^{-3}$ ) or oblique astigmatism ( $Z_2^{-2}$ ), maybe because only 10% of their sample had oblique astigmatism axes. Two different mechanisms have been suggested for this compensation (Artal et al., 2001, Barbero et al., 2002a, Kelly et al., 2004): a passive geometric mechanism resulting from the evolution and genetically programmed, responsible for the compensation of SA, for which the pattern is similar across the population (positive corneal/negative lens SA); and a fine-tuning active process that would take place during the development of the eye (similar to the emmetropisation process for the defocus that will be addressed in section 1.3.-), responsible of the compensation of those aberrations which pattern is more randomly distributed across the population, such as coma and astigmatism. Some years later, Artal et al. (2006) found that eyes with larger misalignments between the fovea and the optical axis, and therefore likely to have larger amounts of coma, had larger coma compensation. He suggested that the passive geometric evolutionary mechanism responsible for SA compensation could also be responsible for coma compensation. Corneal/internal compensation of horizontal coma has also been reported in patients with aspheric intraocular lenses implanted (Marcos et al., 2008), supporting that the mechanism is geometric.

The increased optical aberrations (see section 1.2.4.1.-) present in the old years has been attributed to the loss of this compensation with age, reported for SA. Changes in the crystalline lens seem to be responsible for this balance disruption, as the corneal aberrations have been found to remain fairly constant (Smith et al., 2001).

### 1.2.5.- ABERRATION MEASUREMENT IN PATIENTS: INFLUENCE OF THE MEASUREMENT LIGHT AND SAMPLING PATTERN

The generalised use of aberrometry in clinics has brought some additional needs such as speed in the measurement and comfort for the patient. In applications such as adaptive optics, speed in the data processing is crucial in order to achieve real time correction. Acquisition times can be reduced by reducing the number of samples in sequential aberrometers, or the exposure times. Using infrared (IR) wavelength (more reflected by the eye fundus than visible light (Delori and Pflibsen, 1989)), or polarisation configurations that maximise light reflected on the photoreceptors layer (Lopez-Gil and Artal., 1997) can help to avoid stray light or unwanted reflections in the image, optimising processing time. The latter can also be minimised by decreasing the number of samples. However, given that some aberrometry techniques use light reflected back from the retina, the interaction of the light with the different retinal layers can influence the measured aberration pattern. In addition, changes in the number and distribution of samples can also influence the accuracy in the estimation of aberrations.

#### 1.2.5.1.- Polarisation State of the measurement light

Polarisation is a property of transverse waves that describes the behaviour of the electric field vector  $\vec{E}$  as the wave propagates (see Figure 1.11). When  $\vec{E}$  rotates uniformly through  $2\pi$  radians over one wave period, the wave is said to be elliptically polarised, since the end point of  $\vec{E}$  will describe within each wave period what is called a *polarisation ellipse* (Born and Wolf, 1993) perpendicular to the direction of propagation (Figure 1.11 C). If the modulus of  $\vec{E}$  is constant in time, then the elliptic polarisation will degenerate into circular polarisation (Figure 1.11 B). This happens when the phase difference between the orthogonal components of  $\vec{E}$ ,  $\varphi$ , is an odd multiple of  $\pi/2$ . When  $\vec{E}$  vibrates always on the same plane, the

wave is said to be linearly polarised ( $\delta$  is 0 or a positive multiple of  $\pi$ ) (Figure 1.11 A).

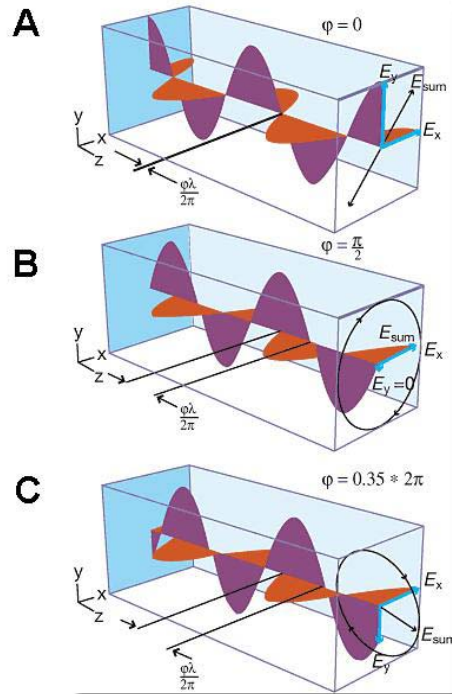


Figure 1.11. Diagrams showing different states of polarisation depending on the behaviour of electric field vector  $\vec{E}$ : linear polarisation (A), circular polarisation (B) and elliptical polarisation (C).  $\varphi$  indicates the phase difference between the x and y components of  $\vec{E}$ . Image obtained from <http://spie.org/x17069.xml?ArticleID=x17069>

There are different ways in which matter interacts with polarised light as it travels through it. The interaction of most importance in the human eye is the retardation due to birefringence. Birefringence results from the existence of two or three different refractive indices in the same material, depending on whether it is uniaxial or biaxial. When light enters a birefringent material, the incident beam is split in two different beams that travel at different speeds (depending on the refraction index they find) and therefore a phase shift will be produced between both components (retardation). When linearly polarised light goes through a birefringent material the phase shift will produce elliptically polarised

light. If the phase shift is  $\pi/2$  (quarter wave plate) the resulting beam will be circularly polarised. Dichroism consists on the selective absorption of light by a material, depending on the propagation direction, and that results in partial polarisation of the light. It is present in the fovea together with birefringence (Van Blokland, 1985).

The cornea, the crystalline lens and the retina interact with polarised light (Van Blokland, 1986, Bueno, 1999, Bour, 1991), producing mainly retardation (Figure 1.12 A). The cornea is the optical element of the eye that most affects polarised light. Corneal epithelium and endothelium (see Figure 1.2) can be considered optically anisotropic. However, the stroma (see section 1.1.1.-), accounting for 90% of corneal thickness, shows birefringence. Although the intrinsic birefringence of the cylindrical collagen fibrils is cancelled out as a consequence of the different orientations of the lattices (Van Blokland and Verhelst, 1987), each lamella shows form birefringence due to the arrangement of the collagen fibrils and can be considered as a retarding plate, with its fast axis aligned with the axis of the collagen fibrils (Farrell et al., 1999). Because there exists a preferential direction in the orientation of the lamellae, usually nasal downwards, the cornea behaves as a biaxial crystal (Van Blokland and Verhelst, 1987), i.e., optically anisotropic in three directions, with the fastest axis lying along the normal to the corneal surface and the slowest axis, parallel to the corneal surface lying usually along the nasal downwards direction (from  $10^\circ$  to  $30^\circ$  from the horizontal). The retardation measured for human corneas varies between  $30^\circ$  to  $90^\circ$ , and increases from the centre to the periphery (Bueno and Jaronski, 2001, Jaronski and Kasprzak, 2003, Gotzinger et al., 2004, Van Blokland and Verhelst, 1987) and in depth (Gotzinger et al., 2004, Van Blokland and Verhelst, 1987). The birefringent structure of the cornea can be seen when the cornea is placed between two crossed polarisers: a typical polarisation cross pattern appears as seen in Figure 1.12 B. The crystalline lens would be expected to show form birefringence due to the structure of the cortex

(Bour, 1991), consisting on a stratified structure of fibre membranes and interstitial cytoplasm (Bettelheim, 1975) arranged like the layers of an onion (See section 1.1.2.-). It also exhibits intrinsic birefringence, probably induced by a regular arrangement of water-insoluble proteins that form the cytoskeletal bodies of its fibre cells (Philipson et al., 1975). However, the contribution of the crystalline lens to the birefringence of the eye is almost negligible, given that intrinsic and form birefringence values are similar in magnitude and of opposed signs, and therefore they cancel each other (Bettelheim, 1975). The retina has been reported to be dichroic as well as birefringent (Bueno, 1999, Hocheimer and Kues, 1982, Naylor and Stanworth, 1954) apparently due to the orientation of the molecules of macular pigment (intrinsic) and the Henle fibres layer (form). A minor contribution from the external segment of the cones to both intrinsic and form birefringence has also been suggested. However, the retardation and the dichroism in the central fovea are quite small.

A mean retardation of  $70^\circ$ , which varied across the pupil, was found experimentally with double-pass ellipsometric measurements ( $\lambda=514$  nm) of the polarization properties of ocular structures (Van Blokland, 1986). This shift will produce an average phase difference of  $\lambda/5$  when changing the polarization of the incident light and/or analyser in the imaging channel in imaging aberrometers. Some HS set-ups described in the literature (Liang et al., 1994) use polarised light in order to avoid corneal reflexes that would make the data processing difficult. The use of polarizers in the illumination and detection channels affects the intensity of the raw data (aerial retinal images captured on a CCD camera). Changes in the polarization state of light passing through the eye produce different intensity patterns after the light passes through an analyzer. These changes of intensity have a large impact on the point-spread-function (PSF) estimates obtained by using a double-pass arrangement that incorporates a polarizing channel and an analyzer channel (Bueno and Artal, 1999). As opposed to the conventional double-pass technique,

the aerial images recorded in LRT or HS systems are used only to compute the centroid of several intensity patterns. However, relative differences in intensity in the core and tails of the retinal image or differences in shape could result in changes in the estimation of the centroid and have an impact on the wave aberration estimate. A previous study (Prieto et al., 2001) using a SRR showed no difference in the wave aberration measured with different states of polarization of the illuminating channel. The possible effect of the polarisation state of the incident and collected light in objective aberrometers (LRT and HS) will be studied in Chapter 3 of this thesis.

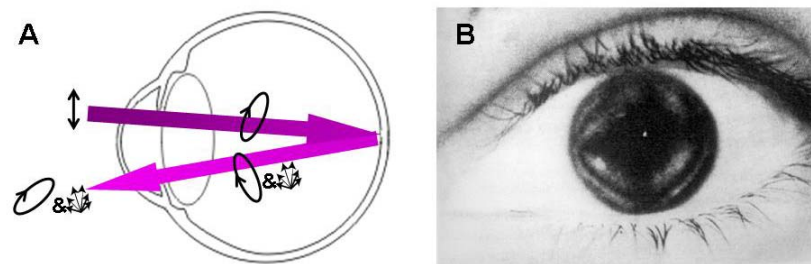


Figure 1.12. Polarisation effects in the eye. (A) Schematic diagram showing the changes that linearly polarised light suffers when it double passes the eye. The corneal and the lens, due to their birefringence, change the light to elliptically polarised. Scattering at the eye fundus produces additional retardation and partial depolarisation. The cornea and the lens introduce additional retardation to the remaining polarised light. Modified from (Van Blokland, 1986). (B) .The corneal polarisation cross. Image from (Cope et al., 1978)

#### 1.2.5.2.- Measurement LightWavelength

Most of the currently available wavefront sensing techniques use IR illumination, due to its advantages over visible light. It is more comfortable for the patient because the human eye is less sensitive to IR (Wysecki and Stiles, 1982); the safety limits for retinal exposure to light are larger in IR range, so more intensities can be applied to the eye (ANSI, 2000); pupil dilation is not strictly required; the retina reflects a higher percentage of the incident light compared with shorter wavelengths (Delori and Burns, 1996); and backscatter by the anterior optics is reduced

(Van Den Berg, 1997). Dynamic measurement (Hofer et al., 2001b, Fernandez et al., 2001) of aberrations is then possible using IR illumination with natural accommodation because mydriasis (and its associated cycloplegic effects, such as paralysation of accommodation) is not necessary. However, given that the visual function takes place under visible light conditions, data from visible light are desirable. For direct comparison between optical measurements (estimated from the wave aberration) and visual performance verification of the equivalence between results obtained with IR light and with visible light is needed. This is particularly important if the measured wave aberration is planned to be used to guide ablation in refractive surgery procedures (see section 1.4.1.-), where the aim is to improve the patient's visual performance. Knowledge of the defocus shift between IR and visible wavelengths is essential if the results are to be used to predict refraction.

It has been reported (Delori and Burns, 1996) that visible light is more likely to be reflected by the photoreceptor outer segments which behave as waveguides (Enoch and Lakshminarayanan, 1991, Marcos and Burns, 1999) whereas near IR light is reflected more by deeper layers RPE and choroid, which backscatter longer wavelengths (Delori and Pfibsen, 1989) (see sections 1.1.4.- and 1.1.5.-). It is also known that the estimation of defocus is affected by the retinal layer in which the light is reflected for the measurement (Howland, 1991). Refraction estimates from retinoscopy are systematically more hyperopic than those from subjective refraction (Safir et al., 1971) and this effect is attributed to the light from the retinoscope reflecting on a retinal layer in front of the photoreceptors (Glickstein and Millodot, 1970). In addition, the longitudinal chromatic aberration (LCA) based on reflectometric double-pass measurements (Rynders et al., 1998, Charman and Jennings, 1976) has been reported to be lower than conventional psychophysical estimates. These findings suggest that reflections at different retinal layers, as well as differences in reflectance and scattering across wavelengths may affect the estimation of

ocular aberrations. They also open the question whether the focus difference can be explained by the LCA and therefore be reasonably predictable across subjects. These questions will be addressed in the study presented in the Chapter 4 of this thesis.

### *1.2.5.3.- Pupil Sampling Pattern*

The actual sampling pattern and density of sampling sub-apertures differ across aberrometers. The lenslets in HS wave aberration sensor are typically arranged in either a fixed rectangular or hexagonal configuration, and the number of samples range from around 50 to more than 15,000 spots within the dilated pupil. Ray tracing aberrometers (such as the LRT or SRR), on the other hand, sample the pupil sequentially and can use a variable sampling configuration. However, given the sequential nature of these devices, high sampling densities are not typically used, to reduce measuring times.

In the case of HS sensor increasing the number of lenslets, and therefore the sampling density, involves: 1) smaller lenslet diameters, which implies a decrease in the amount of light captured by each lenslet and an increase the size of the diffraction-limited spots; 2) greater number of spots, and therefore compromising the dynamic range of the device, as well as an increase of the processing time and potentially decrease the reproducibility, due to the lower signal strengths. In addition, increasing the number of samples may not decrease the variance of the estimates of the wave aberration (Cubalchini, 1979) nor the aliasing error (Soloviev and Vdovin, 2005). For sequential aberrometers, the determination of a sampling pattern with the minimum sampling density providing accurate results is a matter of practical importance, as it decreases measurement time.

The question of the minimum number of samples necessary is of general interest to better understand the trade-offs between aberrometers, but in addition, to study the influence of the sampling pattern will be

useful to determine whether there are sampling patterns that are better adapted to typical ocular aberrations, or particular sampling patterns optimized for measurement under specific conditions. Rectangular and hexagonal distributions are geometries typically used in Hartmann-Shack sensors (Liang et al., 1994, Thibos et al., 1999, Porter et al., 2001, Fernandez and Artal, 2008) or sequential aberrometers (He et al., 1998, Moreno-Barriuso et al., 2001b, Dorronsoro et al., 2003b). However, circular sampling geometries might be more adequate for modal estimation using Zernike coefficients (see section 1.2.2.-), given the circular nature of these functions. Additionally, circular geometry might be more adequate to measure eyes with multifocal contact or intraocular lenses with concentric geometries (Martin and Roorda, 2003, Bennett, 2008). Also, some geometries could be more adequate for specific sampling patterns and need smaller number of samples to accurately retrieve the wave aberration than other geometries.

The first studies on wavefront estimates date from 1979, when Cubalchini (Cubalchini, 1979) was the first to study the modal estimation of the wave aberration from derivative measurements using a least squares method. He concluded that modal estimates of the wavefront obtained using this method, which is almost a standard today in the aberrometry community in combination with the Zernike polynomial series (Rios et al., 1997), were sensitive to the number of samples and their geometry. The problem of the optimal sampling pattern has been investigated theoretically, from both, analytical (Diaz-Santana et al., 2005, Soloviev and Vdovin, 2005) and numerical simulation (He et al., 1998, Burns and Marcos, 2000, Burns et al., 2003) approaches. The findings by previous theoretical studies, described in more depth in chapter 5, section 5.2, can be summarised as follows:

- 1) Number of samples: errors can be minimised by using the minimum number of samples necessary to estimate a fixed number of

Zernike terms (Cubalchini, 1979), and extracting the coefficients corresponding to the maximum complete order possible (He et al., 1998).

2) Spatial distribution of the samples on the pupil: Samples should be taken as far from the centre of the aperture as possible in order to minimise the variance of higher order Zernike terms (McLellan et al., 2006, Applegate et al., 2002, Cubalchini, 1979).

3) Sampling sub-aperture: a sampling aperture size so that the measured extent of the pupil is practically covered minimises the fit error, and the error arising from using the value of the slope at the centre of such large sampling sub-apertures has a small overall effect (He et al., 1998). Using the average slope across the sub-aperture instead of using a point estimator for the derivative at the centre of the aperture decreases modal aliasing (Burns et al., 2003).

4) Sampling patterns (density and distribution): The number of samples and geometry influences modal estimates of the wave aberration by least squares (Cubalchini, 1979). Non-regular distributions seem to perform better in terms of error minimising in presence of sampling noise than regular patterns, such as rectangular or hexagonal grids of similar density (Burns et al., 2003, Diaz-Santana et al., 2005, Soloviev and Vdovin, 2005). Cubatures have been suggested as an example of non-regular sampling schemes (Burns et al., 2003, Rios et al., 1997), and particularly Albrecht cubatures (Bará et al., 1996) have been found to be a good candidate for modal wave aberration reconstruction due to its circular geometry, and greater density in the periphery (Rios et al., 1997). Recent theoretical studies Diaz-Santana et al. (2005) found that the optimal pattern depends on the statistics of the aberration to be measured and the system error, and therefore there is no universal optimal pattern.

The determination of a sampling pattern with the minimum sampling density that provides accurate estimates for the ocular aberrations to be measured is of practical importance for sequential

aberrometers, since it would decrease measurement time, and of general interest to better understand the trade-offs between aberrometers. It is also useful to determine whether there are sampling patterns that are better adapted to typical ocular aberrations, or particular sampling patterns optimized for measurement under specific conditions. Although interesting conclusions have been reached from previous theoretical studies, the applicability to human eyes should be tested experimentally. This question will be addressed in Chapter 5.

#### 1.2.6.- *APPLICATIONS*

Aberrometry has been used to study many different eye-related issues. Some examples are: 1) Ocular aberrations as a function of accommodation (Atchison et al., 1995, He et al., 2000, Hofer et al., 2001a, Plainis et al., 2005) and aging (Calver et al., 1999, Oshika et al., 1999a, Guirao et al., 2000, Mclellan et al., 2001); 2) the study of ametropic eyes (Charman, 2005, Paquin et al., 2002, Radhakrishnan and Charman, 2007, Collins et al., 1995); 3) the assessment of refractive correction techniques such as refractive surgery (Seiler et al., 2000, Moreno-Barriuso et al., 2001b), cataract surgery (Guirao et al., 2002, Barbero, 2003) or contact lenses (Hong et al., 2001, Martin and Roorda, 2003, Dorransoro et al., 2003a); 4) the correction of ocular aberrations to visualize the eye fundus (Liang et al., 1997, Roorda et al., 2002, Burns et al., 2002). In this work aberrometry has been applied to the study of the ametropic eye (myopic and hyperopic eyes), and to the assessment the LASIK corneal surgery as a technique to correct refractive error.

A study of ametropia from an aberrometric approach can contribute to different interesting aspects of research in this topic: 1) Combined measurements of biometry and aberrometry in the same eyes will allow identification of geometrical features leading to given optical properties. 2) Given that the development of myopia and hyperopia are likely substantially different, a comparison between biometry and aberrations in

myopic versus hyperopic eyes may give clues into the development of ametropias. In addition, it has been shown that degraded retinal image quality might lead to elongation of the eye and therefore to myopia, raising the question whether degradation imposed by increased ocular aberrations might lead to development of myopia or increased aberrations in myopic eyes can be a consequence of the structural differences of the myopic ocular components. 3) Knowledge of the optical properties of ametropic eyes (i.e. typical corneal shapes, internal aberrations, etc...) will help in the customisation of correction methods, such as refractive surgery or contact lenses.

On the other hand, aberrometry has shown to be a useful tool to assess objectively the outcomes of Refractive Surgery. Information from both, corneal topography and ocular aberrometry before and after the surgery will also allow: 1) to assess the role of the crystalline lens aberrations in the surgical outcome; 2) to evaluate the changes on the posterior corneal surface and therefore potential role of biomechanical factors; 3) to identify factors related to aberration induction; 4) to understand individual surgical outcomes. 5) to understand better the corneal biomechanics, and to optimise ablation patterns.

### 1.3.- AMETROPIA AND EMMETROPISATION

Ametropia can be defined from the optical point of view as the refractive condition in which best focus for distant objects is not located on the retina of the unaccommodated eye. When best focus is in front of the retina, the eye is said to be myopic, and when it is behind the retina, the eye is hyperopic (see Figure 1.13). Therefore, the image will be perceived as blurred unless the eyes are corrected by refractive means, or in the case of hyperopic eyes, the eye accommodates to bring the image to the retina.

Whereas there is a considerable variation of ocular biometric

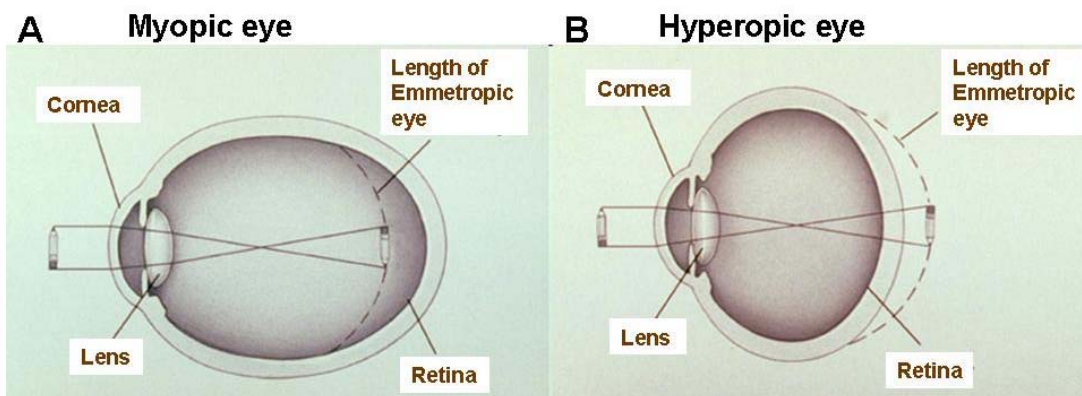


Figure 1.13. Cross-section of ametropic eyes. (A) myopic eye, and (B) hyperopic eye). The main differential feature is the axial length, longer in the myopic eye and shorter in the hyperopic eye, compared to the emmetropic eye, which is used as a reference. Modified from <http://www.drshingorn.com/CSlasik1.htm>

parameters (surface curvatures, distances between components and axial length), each of which following approximately normal distributions (Sorsby et al., 1957, Sorsby et al., 1981, Stenström, 1946 in Charman, 1991b), there is a marked excess of refractions around emmetropia in the population not expectable from a random combination of these parameters. This implies some degree of correlation between the different ocular parameters, which agrees with the observations in the population (Young and Leary, 1991). Straub (1909) called emmetropisation the process that guides the ocular development towards emmetropia (the absence of refractive errors) by adjusting its axial length to the optical power of the

eye, although van Alphen (van Alphen, 1961) owns the credit for the development of the concept (Young and Leary, 1991). The key feature in his theory is that the retinal image quality is continuously monitored at the retinal level, any error signal producing adjustments in axial length. This mechanism has been shown to be visually guided (Wallman, 1993, Wildsoet, 1997, Wallman and Winawer, 2004). Studies using experimental animal eye models show that developing eyes are able to change their structural components (mainly axial length) in order to compensate for the refractive error induced by ophthalmic lenses (Wallman and Winawer, 2004, Schmid and Wildsoet, 1997, Smith and Hung, 1999, Schaeffel and Diether, 1999). In addition, corneal (Gee and Tabbara, 1988) and lens opacities, which make difficult that the retina receives a clear image (Rasooly and BenEzra, 1988), induce excessive eye elongation in infants. While ametropia can be regarded as a failure in the emmetropisation process, the exact cause for the disruption in the eye growth coordination remains unknown. However, the prevalence of myopia related to parental history of myopia seems to point out inheritance has a role in myopia development, and environmental factors related to visual experience (near work, accommodative errors, retinal defocus) seem to be also involved (Gilmartin, 2004, Weale, 2003).

While hyperopia has been usually less studied than myopia because of its smaller prevalence in developed countries, relatively stability and difficulties to measure in young hyperopes (Strang et al., 1998), myopia has attracted even more attention in the last decades. The association of myopia to a greater risk of ocular pathologies, has turned it into an important public health issue (Saw, 2003), specially in Asia and other developed and developing countries where the prevalence has increased in the last decades (Saw, 2003) (Figure 1.14). Prevalence rates are strongly associated to age and genetics (parental myopia, ethnicity) and environmental (near work, school achievement, nutrition) factors: rural areas tend to have a smaller prevalence of myopia than urban areas (Ip et

al., 2008, Saw, 2003), and in terms of ethnicity, high prevalence rates of myopia are found in Chinese and Japanese populations (Saw, 2003). Figure 1.14 shows myopia prevalence and progression in different populations of the world, where the geographical differences are evident in spite of the differences in protocols among studies (Gilmartin, 2004). Most humans are born hyperopic (Wallman and Winawer, 2004), and during the first three years of life (Sorsby et al., 1961) the cornea and the lens have to compensate about 20 D for a 5 mm increase in axial length (AL), adult dimensions being approximately reached at 2 years of age (Gilmartin, 2004). A juvenile phase comes then, between 3 and 13 years of age, where the refractive compensation decreases to about 3 D for about 1 mm increase in AL. Although coordinated biological growth of the eye ceases around 15 years of age, for an important proportion of myopes myopia starts as late as in their early twenties (Gilmartin, 2004).

The significant correlations found between AL and refractive errors points AL out as a major contributor to the refractive state of the eye. In addition, the role of AL in determining the structure of the ocular globe

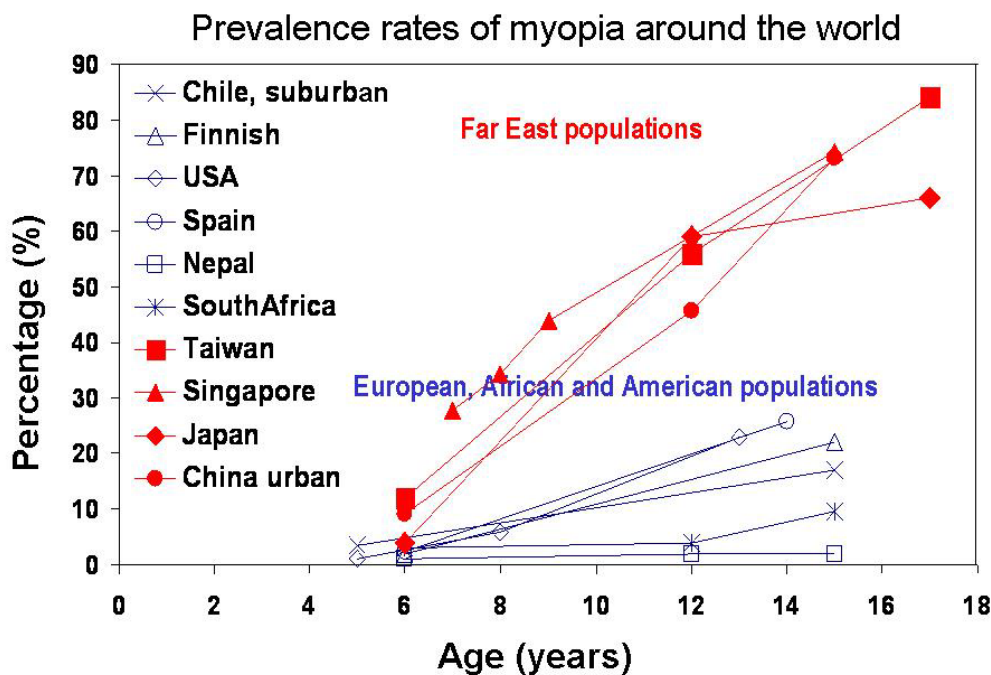


Figure 1.14. Prevalence rates (%) of myopia around the world as a function of age, from (García de la Cera, 2008).

(Sorsby et al., 1961), added to the fact that retinal neurons can be stimulated by hyperopic defocus to release growth factors to enhance scleral growth, thus resulting in an increase of AL (Schaeffel et al., 2003), confirms this as the main variable in the emmetropisation process. This is also supported by the fact that AL has been found to be significantly larger in myopic and smaller in hyperopic eyes than in emmetropic eyes (Strang et al., 1998, Carney et al., 1997, Mainstone et al., 1998, Grosvenor and Scott, 1994). In general, the myopic eye described by the literature (bearing in mind that not all studies agree) is larger than hyperopic or emmetropic eyes in all three dimensions, with a prolate shape (Cheng et al., 1992, Atchison et al., 2004), i.e., more elongated in the axial than in the horizontal and vertical directions (see section 1.1.1.-), apparently due to the constraints imposed by the orbit of the eye (Atchison et al., 2004). This elongation seems to take place at the posterior segment, given that deeper vitreous chambers have been reported for these eyes than for emmetropes (Goss et al., 1997, McBrien and Adams, 1997, Bullimore et al., 1992, Grosvenor and Scott, 1991). Myopic eyes corneas tend to be steeper (smaller anterior CR) than those of hyperopic eyes (Grosvenor and Goss, 1998, Carney et al., 1997, Sheridan and Douthwaite, 1989), and more oblate, i.e., less negative Q values (See section 1.1.1.-) (Carney et al., 1997, Horner et al., 2000, Budak et al., 1999). The crystalline lens power has been reported to be lower in myopic than in emmetropic eyes (Garner et al., 1992, Goss et al., 1997, Weale, 2003), and the anterior chamber deeper in myopic (and emmetropic) eyes than in hyperopic eyes (Weale, 2003).

These structural differences between hyperopic and myopic eyes are likely to determine differences in the optical quality of these eyes. On the other hand, since the emmetropisation process is visually guided, differences in the optical quality of some eyes, and consequent differences in imposed retinal degradation, might play a role in the development of myopia or hyperopia. Knowledge of optical aberrations in the different refractive groups will contribute to develop better correction strategies for

these eyes, but additionally might give some information on the development of ametropia.

### *1.3.1.- AMETROPIA AND OPTICAL ABERRATIONS*

There are not many studies comparing optical aberrations (see section 1.2.4.-) across refractive groups, and the results are somewhat controversial. While some authors did not find a correlation between aberrations and refractive error (Porter et al., 2001, Cheng et al., 2003), or differences in the amount of aberrations across refractive groups (Cheng et al., 2003), other authors reported higher amounts of aberrations in myopes when compared to emmetropes (Collins et al., 1995, He et al., 2002, Paquin et al., 2002, Marcos et al., 2002a). For the SA specifically, some authors find a significant correlation with myopic error (Collins et al., 1995); or significant differences across high myopes with respect to low myopes, emmetropes or hyperopes (Carkeet et al., 2002) while others did not find a significant correlation between SA and a wide range of myopia (Marcos et al., 2002a).

Given that optical aberrations degrade the retinal image quality, and a sharp image is required for proper emmetropisation, a deeper knowledge on the aberration pattern of the ametropic eye, and its relationship with the geometrical structure of the optical components will help to understand possible cause-effect relationships between optical aberrations of the eye and myopia. These effects have been debated both in humans (Thorn et al., 2003) and animal models (de la Cera et al., 2006, Kisilak et al., 2002, Smith, 1998).

## **1.4.- LASIK AS A CORRECTION OF REFRACTIVE ERRORS**

Given that the anterior cornea is the ocular surface that contributes most to the refractive state of eye (Atchison and Smith, 2000) and its easy access, it is not surprising that corneal refractive surgery is currently one

of the most popular surgical approaches to correct ametropia. Incisional corneal surgery first attempts date from 1885 (Sakimoto et al., 2006), and the technique evolved through the 1930s and 40s with Sato (Sato, 1942) to the early 80s when Fyodorov (Fyodorov and Durnev, 1979) developed a systematic more predictable radial keratotomy process that he applied to thousands of patients. In the 1960s, Barraquer (Barraquer, 1964, Barraquer, 1967) invented the Keratomileusis, the first lamellar surgical technique. This technique consisted on separating a thin layer of the superficial corneal tissue using a microkeratome, removing a small piece of cornea, changing its curvature using a lathe, and then suturing it back into place. In the 1980s, Trokel et al. (1983) applied an argon-fluoride excimer laser (with an emission wavelength of 193 nm, which breaks carbon molecules at the corneal stroma) directly on the most external layers of bovine corneas, after previous mechanical removal of the outer layer of the cornea (corneal epithelium) thus giving birth to Photorefractive Keratectomy (PRK). A couple of years later, Seiler (Seiler and Wollensak, 1986) applied for the first time the excimer laser to treat a blind eye to treat ametropia, and in 1989 the first PRK surgery on a myopic seeing eye was performed by McDonald et al. (1989). Munnerlyn et al. (1988) calculated the thickness of tissue necessary to be removed to correct myopia and hyperopia, as a function of the distance to the optical axis. Their suggested ablation pattern included the attempted correction, the radius of curvature of the cornea to be treated, the treatment zone diameter and the corneal refractive index as parameters. However, PRK was limited by unpredictability in higher ranges of refractive error and higher risk of corneal haze after surgery (Corbett et al., 1995). In 1990s Pallikaris (Pallikaris et al., 1990) combined these two techniques (Keratomileusis and PRK), creating the Laser Assisted In situ Keratomileusis (LASIK), which has become the most popular refractive surgery technique. In this technique a hinged flap is created in the cornea by means of a microkeratome (Figure 1.15 B and C), and folded back to let

the stroma exposed (Figure 1.15 D). An excimer laser is then used to photoablate the stroma in the corresponding shape, depending on the kind of treatment (Figure 1.15 E and F). Finally the flap is repositioned in its original place without suturing (Figure 1.15 G). The shape ablation pattern depends on the ametropia to be corrected. In myopic treatment, stromal tissue is removed from the centre of the cornea (Figure 1.16 A) so that the curvature of the central cornea is flattened (Figure 1.16 B), and therefore the excessive refractive power of the myopic eye is compensated. In the case of hyperopic correction the laser removes a ring of tissue in the mid-peripheral zone of the corneal stroma (Figure 1.16 C), resulting in a cone-like corneal profile (Figure 1.16 D), which produces an increased corneal refractive power. The ablation profile in these eyes requires a smooth transition zone to prevent an abrupt step and the peripheral edge (Dierick and Missotten, 1996).

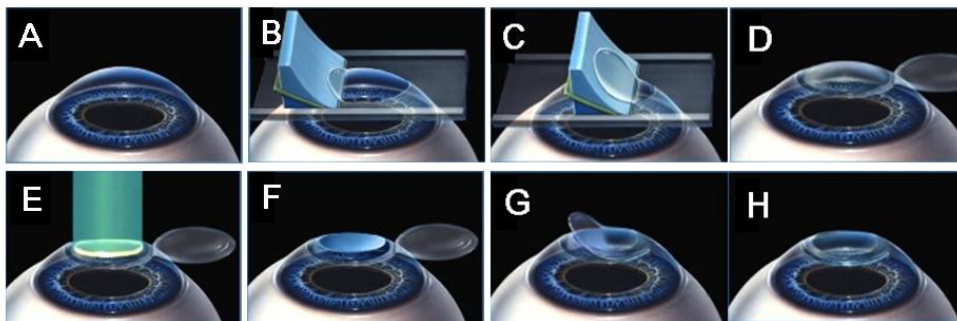


Figure 1.15. LASIK surgical procedure: A hinged flap is created using a microkeratome (B and C), and folded back to let the stroma exposed (D). The stroma is photoablated with an excimer laser in the corresponding shape, depending on the kind of treatment (E and F). Finally the flap is repositioned in its original place without suturing (G and H). <http://www.eyeclinicpc.com>

## LASIK CORRECTION

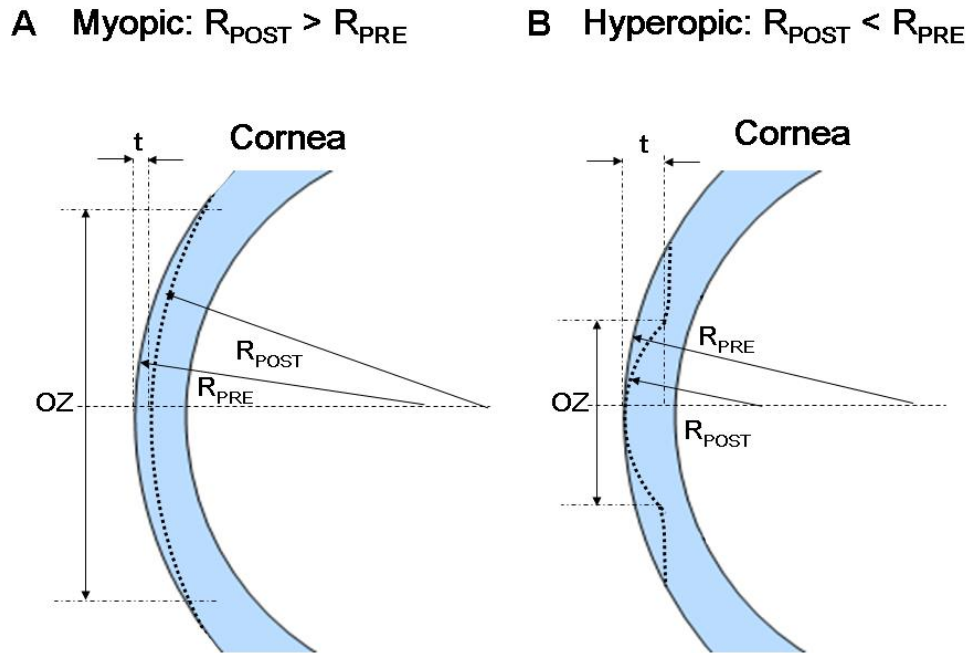


Figure 1.16. Cross-sectional representation of the ablation patterns for myopia and hyperopia correction. In myopic treatment, stromal tissue is removed from the centre of the cornea so that the curvature of the central corneal is flattened (A). In hyperopic correction the laser removes a ring of tissue in the mid-peripheral zone of the corneal stroma, resulting in a cone-like corneal profile (B).  $R_{PRE}$  and  $R_{POST}$  are pre- and post-surgical CR, respectively; OZ stands for optical zone;  $t$  is the maximum thickness ablated in the optical zone. After Munnerlyn et al. (1988).

Although the predictability and accuracy in terms of refraction were quite good in PRK and LASIK within the prescription range suitable for each technique, the patients complained of decreased vision and glare in mesopic and scotopic light levels, i.e., night vision problems. This was illustrated by a decrease in low contrast visual acuity and contrast sensitivity (Verdon et al., 1996, Fan-Paul et al., 2002, Montes-Mico and Charman, 2002). This decrease in visual performance was attributed to haze and scars, and to optical aberrations (Seiler et al., 2000). However, glare disability and decrease in contrast sensitivity do not appear to be correlated with the magnitude of haze after PRK (Seiler et al., 2000), whereas patients with clear corneas also reported these problems (Martinez et al., 1998), and moreover, haze is reduced in LASIK. The fact that optical aberrations are more significant for larger pupils (night vision)

suggests that those are the most likely to be responsible for the reduced visual performance. In fact, the decrease in the area under the contrast sensitivity function has been shown to match the decrease in the area under the modulation transfer function obtained from wave aberrations pointing out at the optical aberrations as the main responsible of post-surgical degradation in the visual performance.

The implementation of aberrometry in refractive surgery has meant a turning point in the history of laser refractive surgery since, along with other technological advances including improvements in surgical lasers (such as flying spot lasers), ablation algorithms and eye-tracking (Mrochen, 2001) the measurement of ocular wave aberrations has opened the potential for improved refractive surgery, aiming not only at correcting refractive errors but also to minimise optical aberrations of the eye.

#### *1.4.1.- REFRACTIVE SURGERY AND OPTICAL ABERRATIONS*

Objective assessment of the optical changes induced by refractive surgery is important to understand the surgical outcomes and optimise corneal laser ablation patterns. Two approaches have been followed, both to assess and to guide ablation procedures: wavefront aberrations, which describe the aberrations of the ocular optical system (Seiler et al., 2000 , Moreno-Barriuso et al., 2001b, Campbell et al., 1999, Thibos et al., 1999), and corneal topography {Applegate R.A., 1998 #1386; Oshika, 1999 #1677; Oliver, 1997 #710; Oliver, 2001 #1379}, which allows to estimate aberrations of the anterior surface of the cornea as well as geometry data (CR and Q). Given that the ablation takes place at the anterior corneal surface, anterior corneal topography seems a suitable tool to assess the outcomes of the surgery. As mentioned above, high correlations between corneal aberrations (wavefront variance) and visual performance (area under contrast sensitivity function) (Applegate et al., 2000) as well as under pre/post- surgical MTF and CSF ratios (Marcos, 2001) have been

reported. However, it is not clear whether aberrations estimated from corneal topography are a sufficient tool to assess optical outcomes, given that even though refractive surgery takes place on the anterior surface of the cornea, the optical properties of this surface are combined with those of the other ocular surfaces to yield the ocular (total) optical quality. Information from both corneal topography and ocular aberrometry is important in understanding individual surgical outcomes, since information of the influence of other optical components of the eye in combination with the cornea on the overall optical quality can be obtained. It also provides insights into the biomechanical response of the cornea (both the anterior and posterior surfaces) to laser refractive surgery, and therefore changes on the posterior surface of the cornea could be assessed.

Published studies on the change of aberrations with refractive surgery for myopia report an increase of total (Seiler et al., 2000, Moreno-Barriuso et al., 2001b) and corneal (Oshika et al., 1999b, Oliver et al., 1997) HOA (i.e. excluding tilts, defocus and astigmatism), mainly due to an increase of SA towards more positive values, although a significant increase in the coma term was also found. Earlier studies of hyperopic correction with excimer laser also suggest an increase of optical aberrations with the procedure. Oliver et al (Oliver et al., 2001) reported a change with PRK in corneal SA from positive in all cases towards negative values and a significant increase in coma RMS. This change in corneal aberrations was greater than that obtained in their previous study on myopic PRK, and consistent with the change in corneal asphericity towards more negative values reported by Chen et al (Chen et al., 2002). Ma et al. (2004) found the greatest RMS and most negative total and corneal SA in their hyperopic LASIK group when compared to their control eyes group and lensectomy group corrected (with intraocular lens implantation) for hyperopia. Additionally, they found significant differences in the internal SA in the LASIK group.

The reported increase in aberrations after surgery, specifically SAs, has driven the advance of corneal refractive surgery due to its impact on postsurgical visual quality. With the insight gained in recent years, the expectations on wavefront-guided procedures have now changed from eliminating to reducing the natural aberrations of the eye, and to minimise the aberrations induced by the procedure (Padmanabhan et al., 2008, Kim et al., 2004, Schallhorn et al., 2008, Kim and Chuck, 2008, Zhang et al., 2008, Netto et al., 2006, Mrochen, 2006). Technological advances (high frequency eye-tracking, improved laser delivery systems, flap creation by femtosecond lasers) (Netto et al., 2006) as well as the greater experience of the surgeons with the platforms available and nomogram optimisation may explain the improvement in the outcomes of wavefront-guided surgery in terms of decrease of induced aberrations reported by more recent studies (Kim et al., 2004, Zhang et al., 2008). Theoretical (Anera et al., 2003, Jimenez, 2004a, Jimenez, 2004b, Kwon et al., 2008, Arba-Mosquera and de Ortueta, 2008) and experimental (Dorransoro et al., 2006) models are being used to identify the different factors that contribute to the induction of the aberrations during the surgery. These different works are being carried out in order to avoid the induction of aberrations by the corneal refractive surgery and they reflect the influence of the experimental work presented in Chapter 6 of this thesis on the evolution of the this field.

## 1.5.- THESIS SYNOPSIS

The body of this thesis is structured as follows:

In **Chapter 2** a description of the common methods used throughout this thesis is given, specifically the laser ray tracing technique used to measure ocular aberrations in subjects. A description of the setup and the control and processing software follows. Finally, some calibrations of the system are reported.

**Chapter 3** presents the study carried out to verify whether the polarisation state of the measurement light used in aberrometry reflectometric techniques (Laser Ray Tracing and Hartmann-Shack) to measure aberrations influences the estimated wavefront. For this purpose, wavefront estimations obtained from different states of light and analyser polarisation are studied as well as the changes in the raw images obtained.

In **Chapter 4** the study performed in order to find out the effect of using IR (786 nm) instead of visible (543 nm) light to measure aberrations using reflectometric techniques is explained. The consistence between the difference in the defocus term with both wavelengths (focus shift) and the shift due to longitudinal chromatic aberration has also been verified. This has important implications for the computation of the refractive error from aberrations measurements.

In **Chapter 5** the effect of applying different patterns to sample the pupil when measuring ocular aberrations on the wavefront estimates is analysed. For this purpose artificial and human eyes were measured using different sampling distributions and densities on the pupil, and the resulting aberrations were studied. In addition numerical simulations were used to extend the extent of the experimental results to abnormal eyes, such as keratoconic or post-surgical eyes.

**Chapter 6** compares optical and biometric properties in two age and refractive error matched groups of myopic and hyperopic eyes, using an optical and geometrical approach. Measurements of anterior corneal and ocular aberrations were performed as well as axial length, and corneal radius and asphericity. The combination of this information gives us an insight on the relationships between the different parameters, as well as the contribution of the crystalline lens to the ocular aberrations.

**Chapter 7** presents the application of ocular and corneal aberrometry to assess the changes produced by LASIK surgery in myopic and hyperopic eyes.

Finally, **Chapter 8** summarises the major findings of this work, and presents a discussion on the implications of the results.